Copy
RM SL54F11

RESEARCH MEMORANDUM

for the

Bureau of Aeronautics, Department of the Navy

LONGITUDINAL STABILITY CHARACTERISTICS OF THE CONSOLIDATED VULTEE XFY-1 AIRPLANE WITH WINDMILLING PROPELLERS AS OBTAINED FROM FLIGHT OF 0.133-SCALE ROCKET-PROPELLED MODEL AT MACH NUMBERS FROM 0.70 TO 1.13

TED NO. NACA DE 369

By Earl C. Hastings, Jr., and Grady L. Mitcham

Langley Aeronautical Laboratory
Langley Field, Va.

NATIONAL ADVISORY COMMITTEE
FOR AERONAUTICS

WASHINGTON

JUN 11 1954

16

NATIONAL ADVISORY COMMITTEE FOR AERONAUTICS

RESEARCH MEMORANDUM

for the

Bureau of Aeronautics, Department of the Navy

LONGITUDINAL STABILITY CHARACTERISTICS OF THE CONSOLIDATED VULTEE XFY-1 AIRPLANE WITH WINDMILLING PROPELLERS AS OBTAINED FROM FLIGHT OF 0.133-SCALE ROCKET-PROPELLED MODEL AT MACH NUMBERS FROM 0.70 TO 1.13

TED NO. NACA DE 369

By Earl C. Hastings, Jr., and Grady L. Mitcham

SUMMARY

A flight test has been conducted to determine the longitudinal stability and control characteristics of a 0.133-scale model of the Consolidated Vultee XFY-1 airplane with windmilling propellers for the Mach number range between 0.70 and 1.13.

The variation of lift-curve slope C_{L_α} with Mach number was gradual with a maximum value of 0.074 occurring at a Mach number of 0.97. Propellers had little effect upon the values of lift-curve slope or the linearity of lift coefficient with angle of attack. At lift coefficients between approximately 0.25 and 0.45 with an elevon angle of approximately -10°, there was a region of neutral longitudinal stability at Mach numbers below 0.93 introduced by the addition of windmilling propellers. Below a lift coefficient of 0.10 and above a lift coefficient of 0.45, the model was longitudinally stable throughout the Mach number range of the test.

There was a forward shift in the aerodynamic center of about 3-percent mean aerodynamic chord introduced by the addition of propellers. The aerodynamic center as determined at low lift moved gradually from a value of 28.5-percent mean aerodynamic chord at a Mach number of 0.75 to a value

of 47-percent mean aerodynamic chord at a Mach number of 1.10. There was an abrupt decrease in pitch damping between Mach numbers of 0.88 and 0.99 followed by a rapid increase in damping to a Mach number of 1.06. The propellers had little effect upon the pitch damping characteristics. The transonic trim change was a large pitching-down tendency with and without windmilling propellers.

The elevons were effective pitch controls throughout the speed range; however, their effectiveness was reduced about 50 percent at supersonic speeds. The propellers had no appreciable effect upon the control effectiveness.

INTRODUCTION

Rocket-propelled-model tests of the Consolidated Vultee XFY-1 airplane are being conducted by the Langley Pilotless Aircraft Research Division at the request of the Bureau of Aeronautics, Department of the Navy. The purpose of this program is to determine the effects of windmilling propellers on the longitudinal and directional stability of the Consolidated Vultee XFY-1 (Phase III) airplane at transonic and low supersonic speeds. The XFY-1 is a modified delta-wing airplane powered with an Allison T-40 gas-turbine engine in combination with a dual-rotating high-speed Curtiss propeller. Longitudinal control is achieved by two control surfaces acting as elevators and roll control is achieved by the same surfaces acting differentially as ailerons. Rudders mounted at the trailing edge of both vertical tails give directional control. The airplane is designed for vertical take-off and transonic speeds after translation into horizontal flight.

A model of this airplane without propellers was tested and is discussed in reference 1. The results presented and discussed herein were obtained from the flight of a 0.133-scale rocket-powered model of the XFY-1 airplane with windmilling propellers. Internal construction of the model tested was such that no space was available for the power unit necessary to duplicate propeller power effects. For this reason, the propellers were allowed to windmill. Data presented in reference 2 show that windmilling has more effect upon the stability data than does the addition of power in the speed range covered by these tests.

In addition to the longitudinal stability and drag data, the effective directional-stability parameter, duct mass-flow ratio, and duct total-pressure recovery are also presented.

SYMBOLS

A	cross-sectional area, sq ft
a_n/g	normal accelerometer reading
b	wing span, ft
$\bar{c}$	wing mean aerodynamic chord, ft
C_c	chord-force coefficient, positive in a rearward direction
C_D	drag coefficient, $C_N \sin \alpha + C_c \cos \alpha$
C_{D_b}	base-drag coefficient, $\frac{-\left(P_{base} - p_o\right) \text{ base area}}{qS}$
$C_{D_{min}}$	minimum drag coefficient
C_h	hinge-moment coefficient, $\frac{\text{Hinge moment}}{qb_e\bar{c}_e^2}$
C_L	lift coefficient, $C_N \cos \alpha - C_c \sin \alpha$
C_m	pitching-moment coefficient about the center of gravity
C_{m_o}	pitching-moment coefficient about the center of gravity at zero angle of attack and elevon deflection
$C_{m_q} + C_{m_{\dot{\alpha}}}$	pitch damping derivatives
C_N	normal-force coefficient, positive toward top of model from model center line
C_{n_β}*	effective rate of change of yawing-moment coefficient with sideslip angle as calculated for a single degree of freedom sideslip oscillation $\frac{4\pi^2 I_Z}{qSb\left(P_{yaw}\right)^2}$
g	acceleration due to gravity, 32.2 ft/sec^2
H	total pressure at duct exit, lb/sq in. abs.

H_o	free-stream total pressure, lb/sq in. abs.
I_Y	moment of inertia about pitch axis, slug-ft^2
I_Z	moment of inertia about yaw axis, slug-ft^2
L	length, ft
$(L/D)_{max}$	maximum lift-drag ratio
m	mass flow through duct, slugs/sec
m_o	mass of air flowing through a stream tube of area equal to the inlet-cowl area under free-stream conditions, slugs/sec
M	Mach number
p_{base}	average base static pressure, lb/sq ft
p_o	free-stream static pressure, lb/sq ft
p_{exit}	duct exit static pressure, lb/sq ft
P	period, sec
q	dynamic pressure, lb/sq ft
R	Reynolds number based on wing mean aerodynamic chord
r	radius of equivalent body of revolution, ft
S	wing area including body intercept, sq ft
$T_{1/2}$	time to damp to one-half amplitude, sec
V	velocity, ft/sec
X	station (measured from nose), ft
α	angle of attack at model center of gravity, deg
β	angle of sideslip at model center of gravity, deg
γ	flight-path angle, deg

δ mean elevon deflection, positive, trailing edge down, deg

θ angle between fuselage center line and horizontal, radians

ρ free-stream mass density of air, slugs/cu ft

Subscripts:

e elevon

$q = \frac{d\theta}{dt}$

cg center-of-gravity location

$C_{m_q} = \frac{dC_m}{d\left(\frac{q\bar{c}}{2V}\right)}$

$\dot{\alpha} = \frac{1}{57.3}\frac{d\alpha}{dt}$

$C_{m_{\dot{\alpha}}} = \frac{dC_m}{d\left(\frac{\dot{\alpha}\bar{c}}{2V}\right)}$

Derivatives are expressed in this manner: $C_{L_\alpha} = \frac{\partial C_L}{\partial \alpha}$; $C_{h_\delta} = \frac{\partial C_h}{\partial \delta}$; and so forth.

MODEL AND APPARATUS

Model

Figure 1 is a three-view drawing of the model tested in this investigation and the physical characteristics of the model are given in table I. The area distribution and equivalent body of revolution are shown in figure 2. This information is included for pressure drag correlation at a Mach number of 1.0. Figure 3 presents the propeller section characteristics as a function of blade station as taken from reference 3. A photograph of the model is shown as figure 4.

The dual-rotating propeller had six Curtiss 1058-1059-XC-4 blades with an NACA 65 airfoil section. For this test the propeller blade angle was 55° at the three-quarter radius. The counterrotating spinners were

made of duralumin and turned independently of each other on bearings located inside the model and on the angle-of-attack sting.

Longitudinal control was provided by a pneumatic system operating two 9.25° swept constant-chord full-span elevons at the trailing edge of the wing. The elevons operated at approximately one square-wave cycle per second between the angles of about -2° and -10° throughout the coasting phase of the flight.

The wings and vertical tails had modified delta plan forms with an NACA 63-009 airfoil section. The wing had 57° of sweepback at the leading edge and an aspect ratio of 1.85. Gun pods and landing struts were located at each wing tip and on the vertical tails. Both wings and vertical tails were made of duralumin plates and spars built up to the proper contour with laminated mahogany.

A choking section (determined by the minimum cross-sectional area of the duct) and an integrating total-pressure tube were installed in the duct exit in order to determine values of internal drag at Mach numbers above 1.0. Because the base of the model tested in this investigation was the same as that of the model tested in reference 1, no base-pressure survey was made of this model.

The model was boosted to low supersonic speeds by a 6.25-inch-diameter Deacon rocket motor. After the booster rocket had stopped thrusting, the model separated from the booster and the data presented herein were obtained during this coasting phase of the flight. The model contained no sustainer rocket motor. Figure 5 is a photograph of the model-booster combination prior to launching.

Apparatus

A telemeter system was used to determine longitudinal stability and drag data. Twelve channels of information were recorded in order to obtain the data presented herein.

The twelve channels of information recorded included angle of attack, angle of sideslip, propeller rotational speed, control position, hinge moment, longitudinal, transverse, and normal accelerations at the center of gravity and normal acceleration at the tail. Three necessary pressure channels were free-stream total pressure, duct-exit total pressure, and static pressure behind the angle-of-attack—angle-of-sideslip flow-direction vane.

A radiosonde released at time of firing recorded free-stream temperature and static pressure. The velocity of the model and its position in space were determined by a CW Doppler radar set and a radar tracking unit.

Ground Tests

In order to obtain the information which was necessary to analyze and correct the data recorded from the flight test properly, several prefiring calibrations were necessary.

Prior to flight testing, the high-speed section of the Langley 7- by 10-foot tunnel was made available for angle-of-attack calibrations for this configuration with and without windmilling propellers. Tests made at Mach numbers of 0.50 and 0.85 indicated that the angle-of-attack vane was located out of the model upwash field for the propellers-off and propellers-on configuration.

The configuration with propellers had counterrotating spinners which turned on several ball bearings fixed directly to the angle-of-attack sting. The wind-tunnel data were also used to determine the amplitude of the oscillations in the angle-of-attack readings which would be fed into the sting by the spinner rotating at high speeds. This effect was found to be negligible.

The model was sting-mounted in the tunnel and tested through an angle-of-attack range of $\pm 4^{\circ}$ with and without windmilling propellers. Instrumentation consisted of an angle-of-attack indicator and a propeller tachometer. Several types of vanes were tested at various distances ahead of the model. Some of the conclusions indicated by an unpublished analysis of these tunnel tests are presented and discussed in the "Accuracy" section of this paper.

Construction of the model was such that there was an inherent looseness in the spinner-bearing assembly which allowed the entire nose to deflect upward about 0.5° under normal load. This movement fed directly into the angle-of-attack—angle-of-sideslip sting and thus to the vane ahead of the model.

Inasmuch as it would have been impossible to remove this motion without reworking the entire bearing assembly, ground calibrations were made to determine the amount of sting deflection due to spinner movements caused by normal loads. These calibrations were made by applying a known load to the spinner assembly at its center of gravity and recording the amount of deflection. Normal accelerations at the center of gravity of the spinner during the flight test were determined by using the recorded values of model normal acceleration and pitching rate at the model center of gravity. The computed nose accelerations were then converted to normal loads and the corresponding deflection applied from the prefiring calibration.

In order to determine the natural frequencies of the model, it was suspended by shock cords and shaken in the pitch plane with an

electromagnetic shaker. Resonant frequencies occurred at 36, 68.5, 110, 134, and 241 cycles per second. The node lines at these frequencies are shown in figure 6.

Several ground calibrations were also necessary in order to correct the recorded elevon angles for twist in the torque rod and aerodynamic loading of the elevon. Reference 1 explains the procedure used in determining the torque rod twist and elevon bending for the model without propellers. The same method was used with this model since the control systems were identical.

ANALYSIS OF DATA

Free oscillations of the model were created by pulsing the elevons in an approximate square-wave motion which resulted in changes in normal acceleration, angle of attack, and hinge moment. The longitudinal-stability analysis of these oscillations is based on two degrees of freedom in pitch, and the directional-stability analysis is based on a single degree of freedom in yaw.

Reference 1 discusses the method of applying the correction for elevon twist and aerodynamic loading on the elevon to the recorded control position and the computation of pitching-moment coefficient by using two normal accelerometers. In the appendixes of references 4 and 5 can be found a more detailed discussion of the methods used in reducing the data from a flight time history to the parameters presented in this paper.

Because the angle-of-attack—angle-of-sideslip indicator is located ahead of the model center of gravity, a correction to the indicated readings was applied for rate of pitch and flight-path curvature as explained in reference 6.

As previously mentioned, this model was instrumented to record lateral force. Lateral oscillations present have been analyzed by the single-degree-of-freedom method of reference 7 where

$$C_{n_\beta}{}^* = \frac{4\pi^2 I_Z}{qSb\left(P_{yaw}\right)^2}$$

The choking section and a total-pressure tube installed in the duct exit made it possible to determine mass-flow ratio, total-pressure recovery, and internal drag based on free-stream and duct exit conditions (see ref. 8). Only one total-pressure tube could be installed because of the

limited number of channels available. For this reason, an integrating tube was used to give an average total-pressure value at the duct exit.

Internal drag was determined by means of the relationship

$$C_{D_{internal}} = \frac{1}{qS}\left[m_{exit}\left(V - V_{exit}\right) - A_{exit}\left(p_{exit} - p\right)\right]$$

Accuracy

Reference 9 presents a discussion of the limitations of the technique and of the accuracy of the measured quantities. In general, the possible instrument errors should be proportional to a certain percentage of the total calibrated range of the instrument.

The maximum possible errors in C_D and C_L presented in the following table were based on an error in angle of attack of 0.5°.

It is felt, however, that this error in angle of attack is larger than should be expected except at lift coefficients near zero where the movement in the spinner bearings allowed the nose to deflect toward the top of the model and thus deflect the angle-of-attack vane 0.5°.

The prefiring calibration discussed previously indicated that for static conditions the spinner assembly could deflect from its neutral position only under the action of positive loads. This condition would occur in flight at small negative normal accelerations. After the spinner assembly had completed 0.5° of travel, further increase in load caused no further deflection. This was a static test with nonrotating spinners. Because of the uncertain action of aerodynamic effects, the corrections applied to the angle of attack due to spinner deflection are not felt to be absolutely correct at lift coefficients near zero where this spinner movement may be taking place.

Therefore, except in the region of lift coefficients near zero, the values of angle of attack are considered to be better than ±0.5° and errors in C_L and C_D are probably not as great as indicated by the following table:

M	ΔC_L	ΔC_D
0.75	±0.033	±0.009
1.10	±.014	±.004

Calculations have shown that an error of $\pm 0.5^{\circ}$ in angle of attack at low lift coefficients could result in very large errors in the values of drag due to lift at subsonic speeds. Because this particular parameter is subject to such large errors introduced by questionable values of angle of attack at low lift coefficients, no values of drag due to lift have been presented in this paper.

RESULTS AND DISCUSSION

The range of Reynolds number and propeller windmilling speed for this test are shown as functions of Mach number in figures 7 and 8, respectively. No positive reason can be advanced for the sudden decreases in propeller speed below $M = 0.85$ but an examination of the flight time history gave no indication of structural failure of any of the blades. An analysis of the propeller speed data during the boosted phase of the flight showed the same abrupt break in the curve at $M = 0.85$. None of the data analyzed showed any large change due to this effect.

Figure 9 presents the supersonic values of duct mass-flow ratio at which this test was conducted. The amount of duct choking was designed to duplicate the inlet-velocity-ratio conditions of the full-scale airplane flying at $M = 0.94$ at approximately 20,000 feet.

Lift

Lift-curve slope.- Figure 10 presents some individual curves of model lift coefficient as a function of angle of attack for various Mach numbers and elevon positions. The breaks in the curves at $M = 0.77$ and $M = 0.87$ in figure 10(a) are a result of the nose movement discussed previously. No lift or angle-of-attack data have been presented in figure 10(a) in the region where nose movement may be occurring.

In figure 10(b) all the lift-coefficient values presented are above the lift region of nose movement indicated by the ground static calibration and therefore are continuous curves.

Figures 10(a) and 10(b) show the lift-coefficient range covered by the test and the linearity of C_L with α at various Mach numbers between $M = 0.70$ and $M = 1.13$. There are no unusual variations of C_L with α and the curves show the same general shape as the data from the configuration without propellers reported in reference 1.

The variation of lift-curve slope C_{L_α} with Mach number is shown in figure 11. These values were taken over the linear lift range for both the low and high elevon settings. Wind-tunnel values from the test

of this configuration with windmilling propellers (ref. 3) are presented for comparison. The agreement is considered to be generally good.

Values of lift-curve slope for $\delta \approx -2^{\circ}$ increase gradually from 0.048 at $M = 0.70$ to a maximum of 0.074 at $M = 0.97$ and then decrease gradually to 0.061 at $M = 1.13$. The lift-curve slope in the high trim lift region is shown by the curve for $\delta \approx -10^{\circ}$ in figure 11. At Mach numbers below $M = 0.93$, the increase in the trim lift range reduces the value of lift-curve slope about 0.010 at $M = 0.75$ and 0.015 at $M = 0.90$. Above $M = 0.93$, there were no high lift data obtained.

Comparison of the individual curves of C_L against α and C_{L_α} against Mach number as determined from this test with the propellers-off test of reference 1 shows the effect of propellers on these lift characteristics. There was no appreciable change in the linearity of C_L with α and very little change in the lift-curve slope introduced by the addition of windmilling propellers to the basic configuration.

Buffet.- Throughout the flight there were small amplitude oscillations in the normal-acceleration and angle-of-attack channels at exactly the same frequency as the propeller speed. The wind-tunnel calibrations and experience with a dummy model with this spinner assembly mounted on a booster had shown that these oscillations were probably due to motion imparted to the model by dynamic propeller unbalance.

At the higher lift coefficients, however, there were some larger amplitude oscillations of a random nature which diminished as the angle of attack decreased as shown in figure 12. Although it is believed that this condition is indicative of buffet, the combination of the two motions made it difficult to determine the point at which the buffet intensity rise occurred. For this reason, no buffet data have been presented in this paper even though it is felt that some buffet is present. The tests with the propellers-off model of reference 1 also showed the presence of buffet at the higher lift coefficients.

Wing dropping.- No values of wing-tip helix angle $pb/2V$ are presented because an analysis of the data showed that the rate of roll for the model was small (0 to 0.3 radian/sec) and random in nature. There was no indication of serious wing dropping from the test.

Drag

Minimum drag.- The minimum drag coefficients presented herein include both internal and base drag and were taken from lift-drag polars plotted from the flight data. Figure 13(a) presents minimum drag coefficient as a function of Mach number for the model with windmilling propellers and

the model of reference 1 and figure 13(b) shows base drag throughout the speed range and internal drag at Mach numbers greater than 1.0. Internal and base drag are presented for tare corrections because the internal ducting and the base of the model did not duplicate the full-scale airplane.

The minimum drag coefficient with $\delta \approx -2^\circ$ varies gradually from a value of 0.023 at $M = 0.70$ to a value of 0.053 at $M = 0.95$ and then increases rapidly to 0.095 at $M = 1.00$. Above this Mach number the drag coefficient gradually increases to a value of 0.099 at $M = 1.12$. At Mach numbers between $M = 0.60$ and $M = 0.70$, $C_{D_{min}}$ with $\delta \approx -2^\circ$ remains constant at $C_D = 0.022$.

The unusual shape of the minimum drag curve is attributed to the early drag rise of the propellers which are operating at a Mach number greater than free stream. Another factor introduced by the propellers is a region of reduced Mach number and dynamic pressure behind the propellers in which the model wing operates. The critical Mach number of the wing in this retarded-flow region could account for the abrupt increase in drag at $M = 0.97$.

Base drag.- Figure 13(b) shows the model base drag coefficient from $M = 0.75$ to $M = 1.13$. This coefficient was determined from the flight of the model without propellers and is discussed in more detail in reference 1. Inasmuch as the base of the model discussed herein was the same as the base of the model of reference 1, the base drag was merely assumed to be the same and is presented in figure 13(b). The base drag coefficient varied from about $C_{D_{base}} = -0.001$ at subsonic speeds to $C_{D_{base}} = 0.002$ at supersonic speeds.

Internal drag.- The internal drag coefficient at Mach numbers greater than 1.0 is also presented in figure 13(b). The value is constant at 0.001 from $M = 1.0$ to $M = 1.13$. Previous experience has shown that there is little change in internal drag between subsonic and supersonic speeds.

Hinge Moments

The hinge-moment characteristics of the elevon in the form of the variation of hinge-moment coefficient with elevon deflection C_{h_δ} and the variation of hinge-moment coefficient with angle of attack C_{h_α} are given as functions of Mach number in figures 14 and 15. These figures show the data points obtained and are only partially faired since it is felt that there are insufficient data presented to establish definitely the shape of the curves. The data points for C_{h_δ} shown in figure 14 have the same general variation with Mach number as the propellers-off test points of reference 1, which are presented for comparison.

Comparison of the values of C_{h_α} shown in figure 15 with those of reference 1 shows good agreement below $M = 0.90$ and at approximately $M = 1.1$.

Static Longitudinal Stability

The static longitudinal stability characteristics of the model are shown in figures 16 and 17. Figure 16 shows the basic pitching-moment data as the variation of pitching-moment coefficient with lift coefficient. All moment data were taken about the center of gravity at $0.14\bar{c}$. The values of pitching-moment coefficient presented were obtained by using two accelerometers and applying the method of reduction discussed in reference 1. Figure 16(a) shows pitching-moment coefficient C_m as a function of lift coefficient C_L in the low trim lift region with an elevon deflection of approximately -2° at various Mach numbers. Over the low-lift range covered at this elevon setting, C_m varies linearly with C_L except at $M = 0.75$ where some nonlinearity may be indicated above $C_L = 0.10$.

The basic pitching-moment data in the high lift region are shown in figure 16(b) where C_m is plotted against C_L for $\delta \approx -10^\circ$. At supersonic speeds, no high trim lift data were obtained because of the increase in static stability and the reduction of elevon effectiveness but the nonlinearity of C_m with C_L can be seen below a Mach number of 1.03. At $M = 0.93$, C_m is nonlinear with C_L over the range of C_L presented. Neutral stability was indicated between about $C_L = 0.25$ and $C_L = 0.45$ at Mach numbers below $M = 0.93$. Above $C_L = 0.45$ at $M = 0.82$ and $M = 0.73$ the model is longitudinally stable, although the pitching-moment curve is nonlinear at $M = 0.73$. Wind-tunnel tests of this configuration with windmilling propellers (ref. 3) were made at the same center-of-gravity location as the rocket model. These tests show that, from $M = 0.85$ to $M = 0.93$, C_m is nonlinear with C_L over the entire lift range of the tunnel test (about $C_L = -0.05$ to $C_L = 0.75$). At Mach numbers of 0.90 and above, the tests of reference 3 show the region of neutral or negative longitudinal stability to be between $C_L = 0.05$ and $C_L = 0.22$. These tests, however, were made with $\delta = 0^\circ$ and the data presented herein indicate that the difference in the range of lift coefficient for neutral stability could be caused by the difference in elevon angles for the two tests.

The aerodynamic-center location of the model tested in this investigation is shown as a function of Mach number in figure 17. These values were determined by using the slopes of the linear portions of the pitching-moment curves presented in figure 16(a). The aerodynamic center as determined in the low trim lift region ($-0.20 < C_L < 0.10$) moves gradually from

28.5-percent mean aerodynamic chord at $M = 0.75$ to 46.5-percent mean aerodynamic chord at $M = 1.10$.

Comparison of the pitching-moment and aerodynamic-center data presented in figures 16 and 17 with the data of reference 1 (same configuration tested at the same center of gravity but without propellers) will show the effects of propellers on the longitudinal stability characteristics of these models.

In the high lift region of the tests the model without propellers had nonlinear pitching-moment curves at $M = 0.86$ and below, whereas the addition of propellers caused the model to be neutrally stable longitudinally below $M = 0.93$ between $C_L \approx 0.25$ and $C_L \approx 0.45$. The aerodynamic-center locations for the two models as determined from the low lift range of the tests show that the model tested with windmilling propellers has an aerodynamic-center location approximately 3.0 percent of the mean aerodynamic chord farther forward than the model without propellers at subsonic speeds and 4.5 percent farther forward at supersonic speeds.

Damping in Pitch

The short-period longitudinal oscillations which occurred during the flight as a result of abrupt control movements were analyzed by the method of reference 4 to obtain damping data. The damping-in-pitch characteristics of the model are given by the parameters, the time required to damp to half amplitude and $C_{m_q} + C_{m_{\dot{\alpha}}}$, which are presented as functions of Mach number in figures 18 and 19, respectively. Figure 19 shows that the pitch-damping parameter $C_{m_q} + C_{m_{\dot{\alpha}}}$ decreases rapidly from $M = 0.88$ to $M = 0.99$ and then shows a rapid increase to $M = 1.06$. This phenomenon of a sudden decrease in pitch damping followed by an abrupt increase has been observed on other triangular wings and in the test of this configuration without propellers which is shown for comparison in figure 19. Reference 10 discusses the damping in pitch on some low-aspect-ratio wings.

Longitudinal Control Effectiveness

Control effectiveness parameters in the form of rate of change of lift coefficient with elevon deflection C_{L_δ} and rate of change of pitching-moment coefficient with elevon deflection C_{m_δ} are presented as functions of Mach number in figures 20 and 21, respectively.

Control lift effectiveness C_{L_δ} decreases gradually from a value of 0.014 at $M = 0.75$ to a value of 0.007 at $M = 1.10$. Variation of the pitching effectiveness C_{m_δ} is gradual; C_{m_δ} decreases from a value of 0.008 at $M = 0.75$ to a value of -0.003 at $M = 1.10$.

A comparison of these parameters with those reduced from the flight test of the model without propellers will show that the control-effectiveness values are relatively unaffected by adding propellers. The values of C_{L_δ} and C_{m_δ} presented in figures 20 and 21 also indicate that the elevon is an effective control for producing lift and pitching moments throughout the Mach number range of this test, although the effectiveness is reduced at the higher Mach numbers.

Trim Lift Coefficient

The model trim lift coefficient is shown in figure 22 for several elevon positions over the Mach number range of the test. For the smaller elevon positions, the model trims at lift coefficients between -0.060 and -0.110 throughout the test. For the larger elevon positions, the model trims at about $C_{L_{trim}} = 0.34$ at subsonic speeds and $C_{L_{trim}} = -0.03$ at Mach numbers between $M = 1.00$ and $M = 1.08$ with a rapid decrease in $C_{L_{trim}}$ occurring between $M = 0.88$ and $M = 1.00$. Because of the nonlinearity of the pitching-moment curves in the high lift region, the use of extrapolation between the curves shown in figure 22 should be exercised with caution.

Longitudinal Trim

The basic pitching-moment coefficient C_{m_o} at zero elevon deflection and zero angle of attack is shown in figure 23. Values taken from the test without propellers are presented for comparison. Values of C_{m_o} are negative throughout the speed range for both configurations and vary from a value of -0.017 at $M = 0.73$ to a value of -0.063 at $M = 1.13$ with windmilling propellers. The variation with Mach number is gradual for the propellers-on test whereas it is abrupt for the propellers-off test.

Static Directional Stability

Oscillations present in the angle-of-sideslip flight time history were analyzed to determine the rate of change of effective yawing-moment coefficient with sideslip C_{n_β}*. This parameter is presented as a function

of Mach number in figure 24 and wind-tunnel values, as shown in reference 3, are presented for comparison. The values of C_{n_β}* obtained from this test with propellers increase from C_{n_β}* = 0.0033 at M = 0.73 to a maximum of C_{n_β}* = 0.0085 at M = 1.05 and remain fairly constant to M = 1.13. Agreement with the wind-tunnel data is considered generally good. The maximum angle of sideslip of the model β was approximately $\pm 4^\circ$. The effect of the addition of windmilling propellers can be seen by comparison with the propellers-off data which are also presented in figure 24. There is an increase in C_{n_β}* of 0.0026 at M = 0.75 and 0.0030 at M = 1.10 introduced by the addition of propellers.

This method of analysis is based on a single degree of freedom in yaw and assumes that C_n is linear with β. This assumption is considered to be satisfied in this analysis on the basis of the directional-stability data presented in reference 3. These data indicate that linearity exists between the β limits of $\pm 4^\circ$ at high subsonic speeds.

Duct Total-Pressure Recovery

An integrating total-pressure tube was installed at one duct exit to determine the internal drag of the duct at Mach numbers greater than 1.0. Inasmuch as previous experience has shown that the total-pressure losses through a short duct of this type are small, the total pressure at the exit should not be greatly different from that at the inlet. For this reason, the ratio of the total pressure recorded at the exit to the total pressure of the free stream is thought to be of importance because of its similarity to inlet total-pressure recovery and is presented as figure 25. The duct total-pressure recovery decreases gradually from 0.86 at M = 1.00 to 0.77 at M = 1.13.

CONCLUSIONS

Results from the flight test of a 0.133-scale model of the Consolidated Vultee XFY-1 airplane with windmilling propellers from Mach number 0.70 to Mach number 1.13 indicate the following conclusions:

1. The addition of windmilling propellers to the basic configuration has very little effect upon the lift-curve slope. The lift-curve slope varies gradually with Mach number, a maximum value of 0.074 occurring at a Mach number of 0.97.

2. The minimum drag coefficient at an elevon position of approximately -2° varies from a value of 0.023 at a Mach number of 0.71 to a

value of 0.053 at a Mach number of 0.97. There is then an abrupt increase in minimum drag coefficient to 0.095 at a Mach number of 1.00 followed by a gradual increase to 0.099 at a Mach number of 1.12.

3. The addition of propellers resulted in a region of neutral longitudinal stability between lift coefficients of about 0.25 and about 0.45 below a Mach number of 0.93 when the elevon angle was approximately -10°. Above a lift coefficient of 0.45, the model was longitudinally stable, although at a Mach number of 0.73 the pitching-moment curve was nonlinear.

4. The addition of windmilling propellers to the basic configuration caused a forward shift of about 3-percent mean aerodynamic chord in the aerodynamic-center location as determined at low lift. The aerodynamic center with an elevon position of approximately -2° moves gradually from a location of 28.5-percent mean aerodynamic chord at a Mach number of 0.75 to a position of 47-percent mean aerodynamic chord at a Mach number of 1.10.

5. There is an abrupt decrease in pitch damping between Mach numbers of 0.88 and 0.99, followed by a rapid increase in damping to a Mach number of 1.06. There were no large changes in the pitch damping characteristics introduced by the addition of windmilling propellers.

6. The transonic trim change is a large pitching-down tendency with and without propellers. The pitching-moment coefficient at zero angle of attack and elevon deflection with windmilling propellers varies from a value of -0.018 at a Mach number of 0.73 to a value of -0.060 at a Mach number of 1.13.

7. The elevon is an effective control in producing lift and pitching moment throughout the test Mach number range. At supersonic speeds the control effectiveness is reduced to about one-half its subsonic value. The propellers have no appreciable effect upon the control effectiveness.

Langley Aeronautical Laboratory,
National Advisory Committee for Aeronautics,
Langley Field, Va., June 2, 1954.

Earl C. Hastings, Jr.
Earl C. Hastings, Jr.
Aeronautical Research Scientist

Grady L. Mitcham
Grady L. Mitcham
Aeronautical Engineer

Approved:
Joseph A. Shortal
Joseph A. Shortal
Chief of Pilotless Aircraft Research Division

mhg

REFERENCES

1. Hastings, Earl C., Jr., and Mitcham, Grady L.: Flight Determination of the Longitudinal Stability Characteristics of a 0.133-Scale Rocket-Powered Model of the Consolidated Vultee XFY-1 Airplane Without Propellers at Mach Numbers From 0.73 to 1.19 - TED No. NACA DE 369. NACA RM SL54B03a, Bur. Aero., 1954.

2. Sutton, Fred B., and Buell, Donald A.: The Effect of an Operating Propeller on the Aerodynamic Characteristics of a 1/10-Scale Model of the Lockheed XFV-1 Airplane at High Subsonic Speeds - TED No. NACA DE 377. NACA RM SA52E06, Bur. Aero., 1952.

3. Wall, P. J.: A Preliminary Analysis of the First Series of High-Speed Wind Tunnel Tests of the Convair Model 5 Airplane. Aero. Memo. No. A-5-27, Consolidated Vultee Aircraft Corp., Mar. 3, 1952.

4. Mitcham, Grady L., Stevens, Joseph E., and Norris, Harry P.: Aerodynamic Characteristics and Flying Qualities of a Tailless Triangular-Wing Airplane Configuration As Obtained From Flights of Rocket-Propelled Models at Transonic and Low Supersonic Speeds. NACA RM L9L07, 1950.

5. Gillis, Clarence L., Peck, Robert F., and Vitale, A. James: Preliminary Results From a Free-Flight Investigation at Transonic and Supersonic Speeds of the Longitudinal Stability and Control Characteristics of an Airplane Configuration With a Thin Straight Wing of Aspect Ratio 3. NACA RM L9K25a, 1950.

6. Mitchell, Jesse L., and Peck, Robert F.: An NACA Vane-Type Angle-of-Attack Indicator for Use at Subsonic and Supersonic Speeds. NACA RM L9F28a, 1949.

7. Bishop, Robert C., and Lomax, Harvard: A Simplified Method for Determining From Flight Data the Rate of Change of Yawing-Moment Coefficient With Sideslip. NACA TN 1076, 1946.

8. Faget, Maxime A., Watson, Raymond S., and Bartlett, Walter A., Jr.: Free-Jet Tests of a 6.5-Inch-Diameter Ram-Jet Engine at Mach Numbers of 1.81 and 2.00. NACA RM L50L06, 1951.

9. Gillis, Clarence L., and Vitale, A. James: Wing-On and Wing-Off Longitudinal Characteristics of an Airplane Configuration Having a Thin Unswept Tapered Wing of Aspect Ratio 3, as Obtained From Rocket-Propelled Models at Mach Numbers From 0.8 to 1.4. NACA RM L50K16, 1951.

10. Tobak, Murray: Damping in Pitch of Low-Aspect-Ratio Wings at Subsonic and Supersonic Speeds. NACA A52L04a, 1953.

TABLE I

PHYSICAL CHARACTERISTICS OF A 0.133-SCALE MODEL

OF THE CONSOLIDATED VULTEE XFY-1 AIRPLANE

Wing:	
Area (included), sq ft	6.31
Theoretical span, ft	3.42
Aspect ratio (based on theoretical span)	1.85
Mean aerodynamic chord, ft	2.09
Sweepback of leading edge, deg	57
Sweepback of trailing edge, deg	9.25
Dihedral (relative to mean thickness line), deg	0
Taper ratio (theoretical tip chord/root chord)	0.22
Airfoil section	modified NACA 63-009
Vertical Tail:	
Area (included), sq ft	3.13
Span, ft	3.19
Aspect ratio	3.25
Sweepback of leading edge, deg	40
Sweepback of trailing edge, deg	6
Taper ratio (theoretical tip chord/root chord)	0.40
Airfoil section	modified NACA 63-009
Elevon:	
Total area (back of hinge line), sq ft	0.57
Chord (perpendicular to hinge line), ft	0.24
Total span, ft	1.32
Propeller:	
Number of blades	6
Diameter, ft	2.14
Blade angle at 0.75 radius, deg	55
Airfoil section at 0.75 radius	NACA 65-707
Ducts:	
Inlet area of each duct, sq in.	2.75
Exit area of each duct, sq in.	1.77
Weight and Balance:	
Weight, lb	212.0
Wing loading, lb/sq ft	33.6
Center-of-gravity location, percent $\bar{c}$	14.0
Moment of inertia in pitch, slug-ft^2	9.80
Moment of inertia in yaw, slug-ft^2	10.33

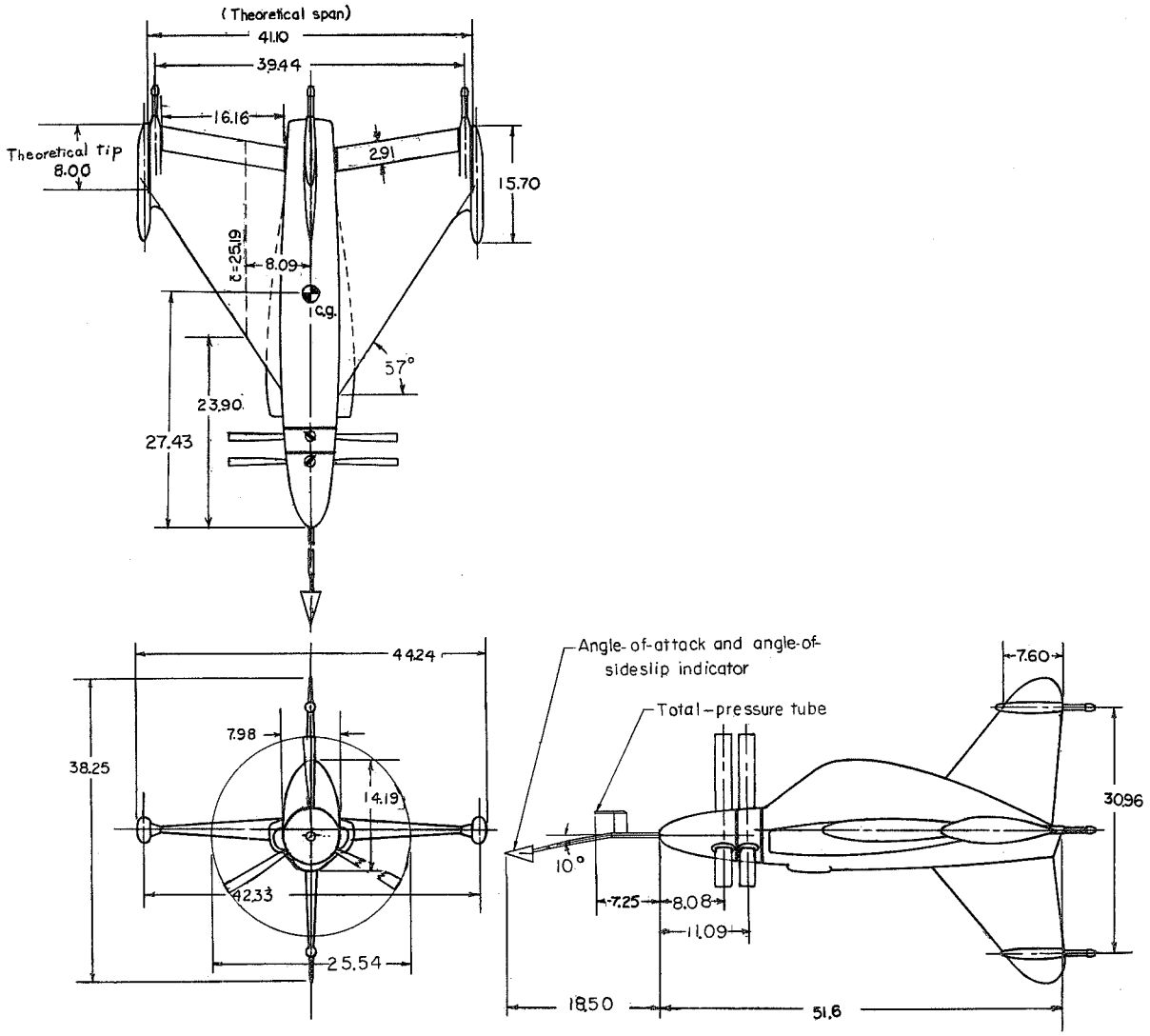

Figure 1.- Three-view drawing of the model. (All dimensions are in inches.)

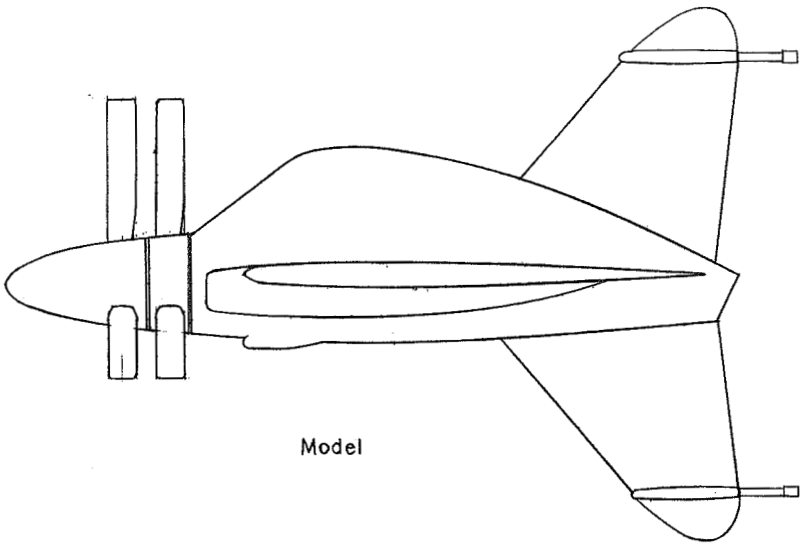

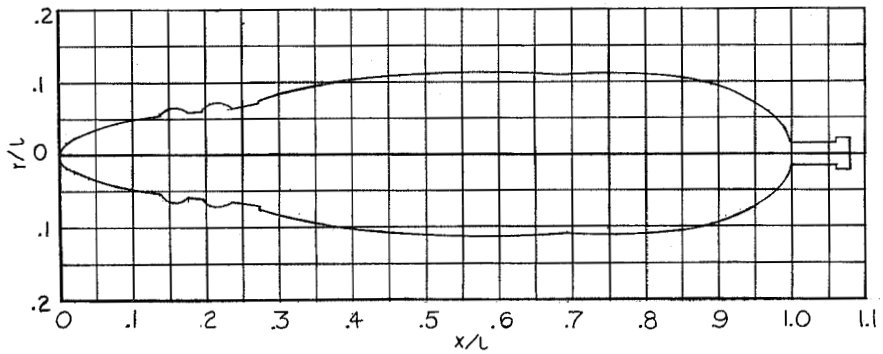

(a) Equivalent body of revolution.

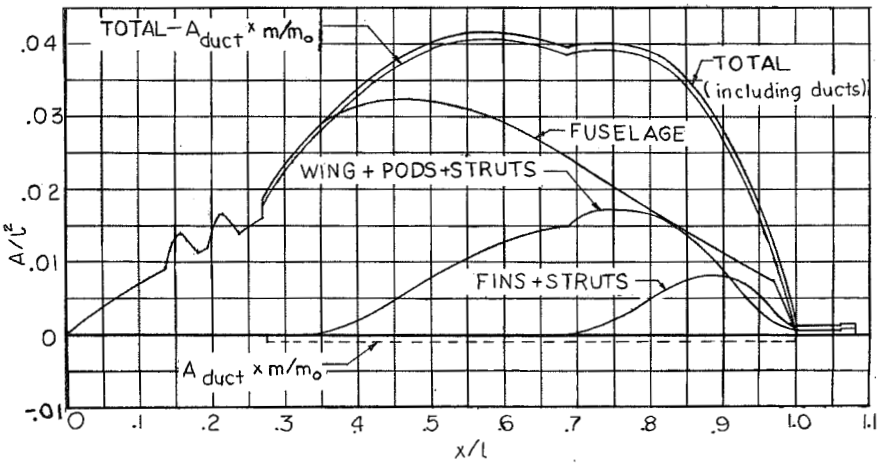

(b) Area distribution.

Figure 2.- Area distribution and equivalent body of revolution of the model.

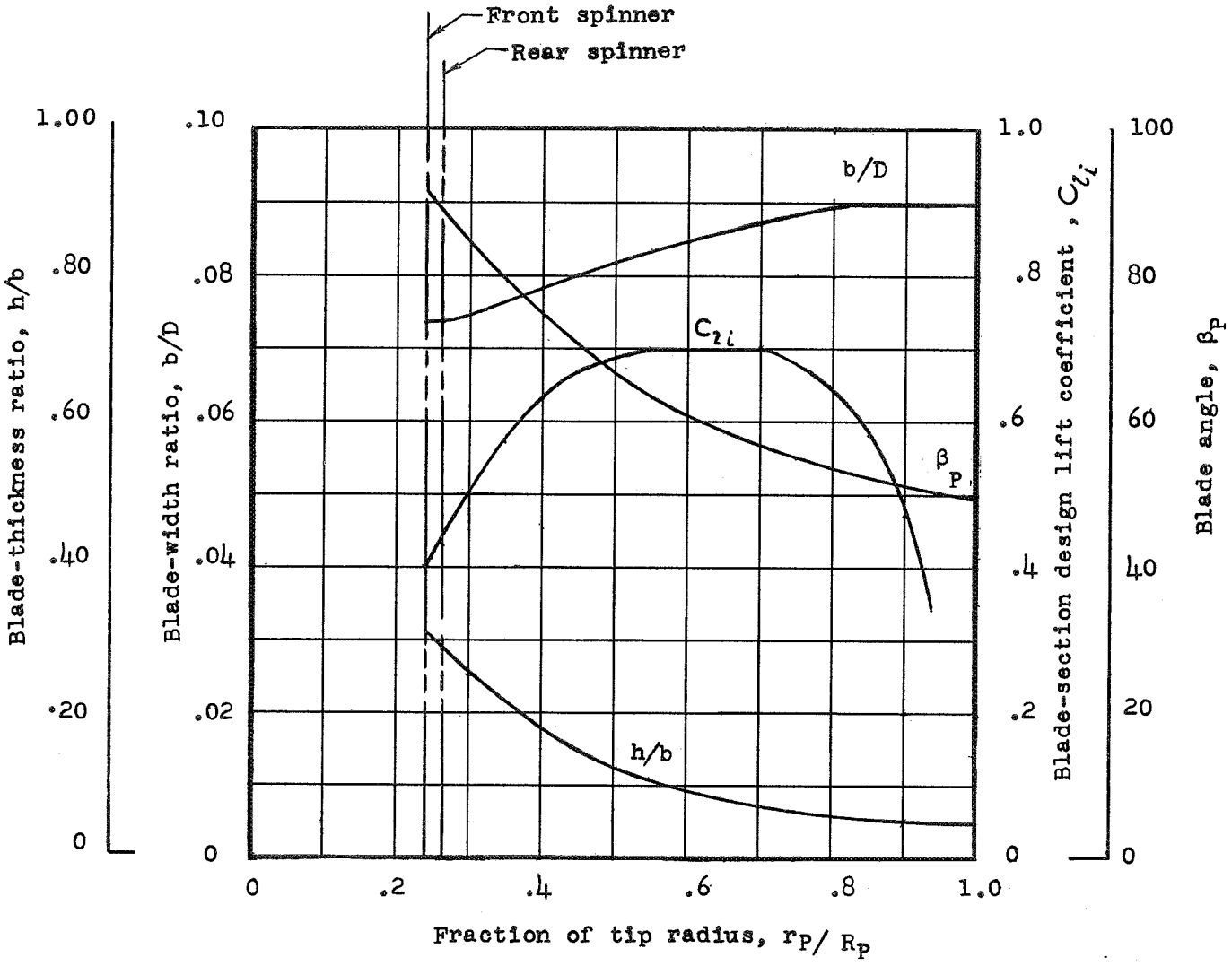

Figure 3.- Plan-form and blade-form curves for the Curtiss 1058-1059-XC-4 dual-rotating propeller.

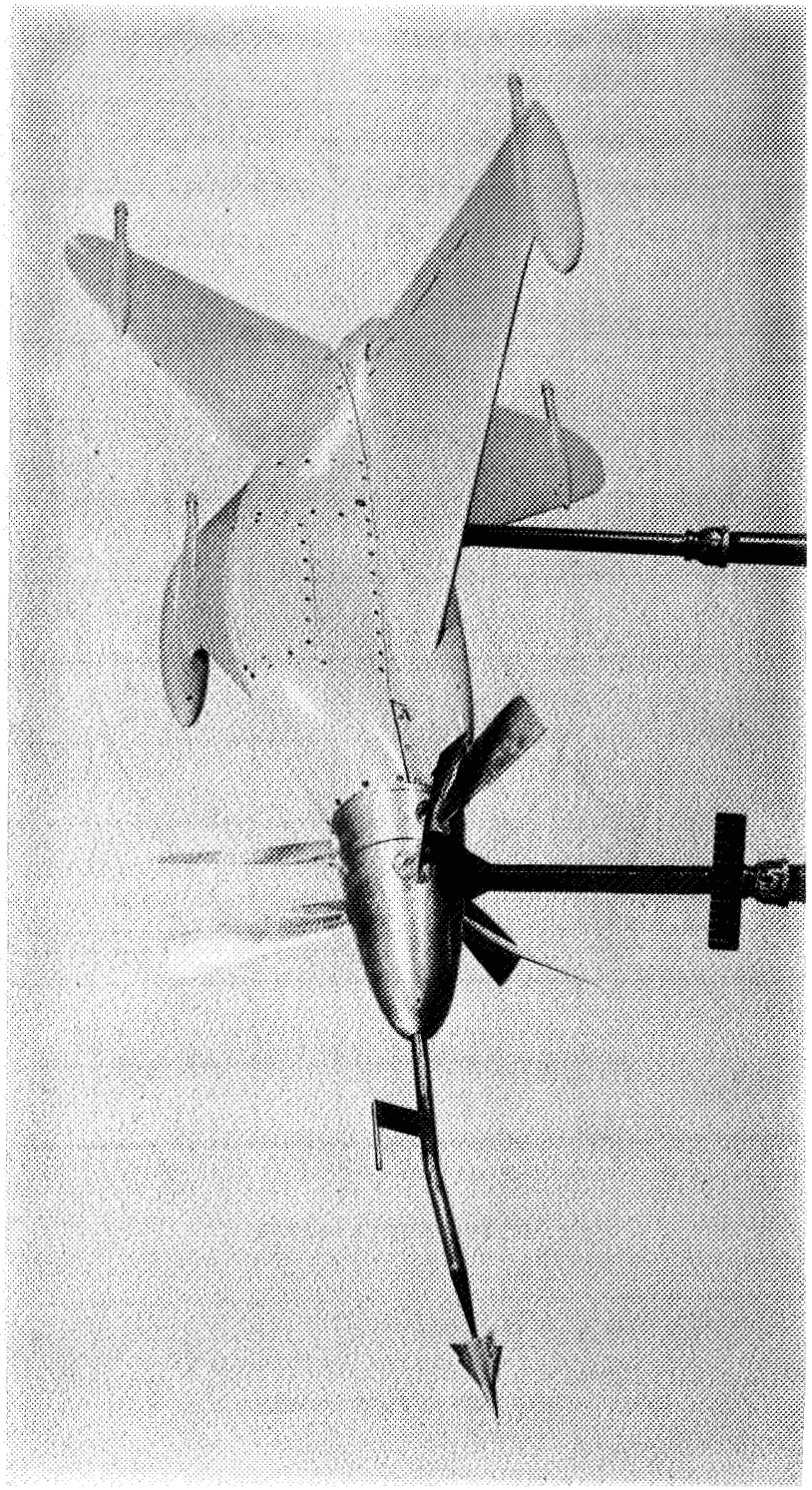

L-81953.1

Figure 4.- Photograph of the model.

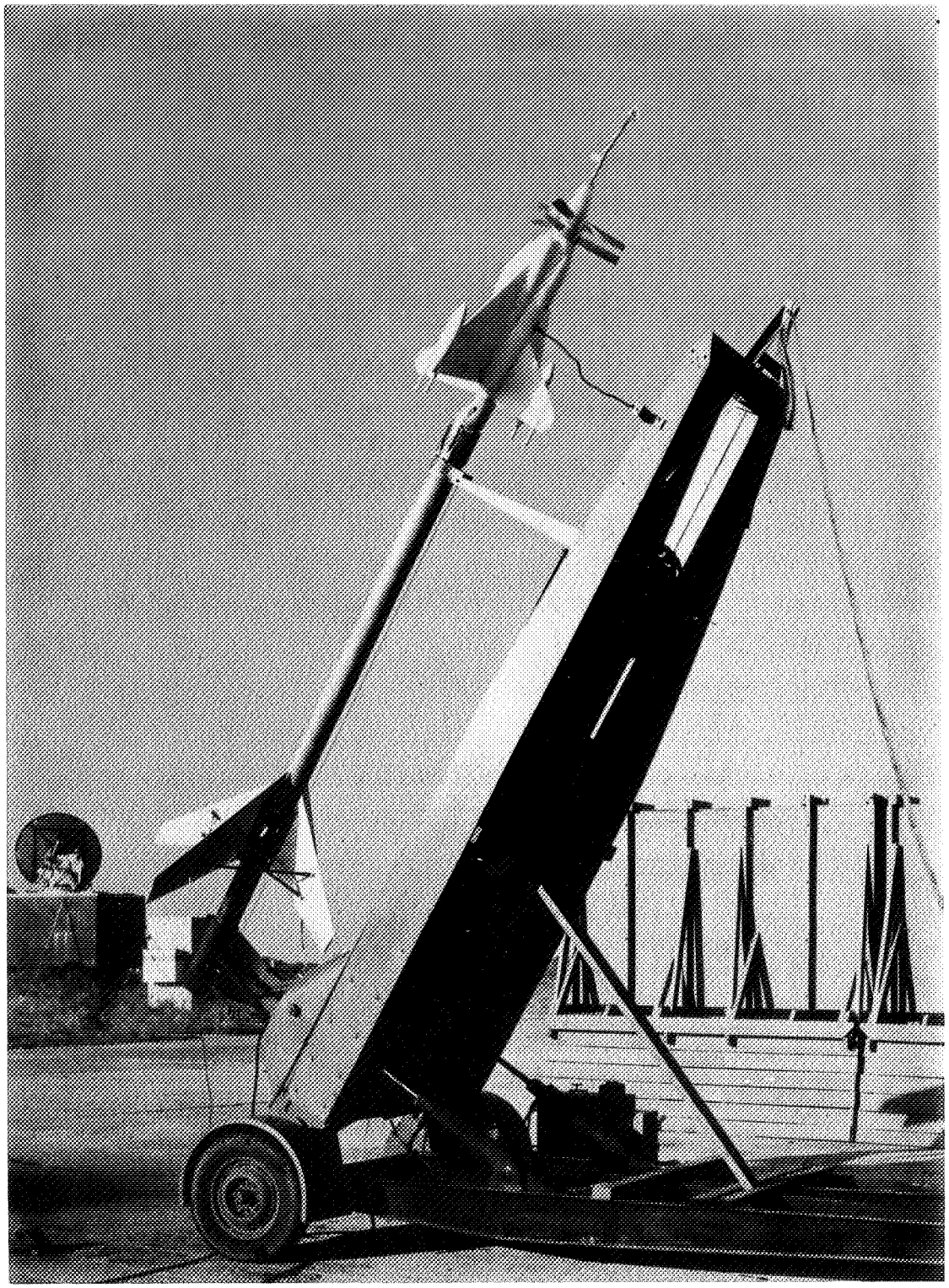

L-82358.1

Figure 5.- Booster-model combination on the launcher.

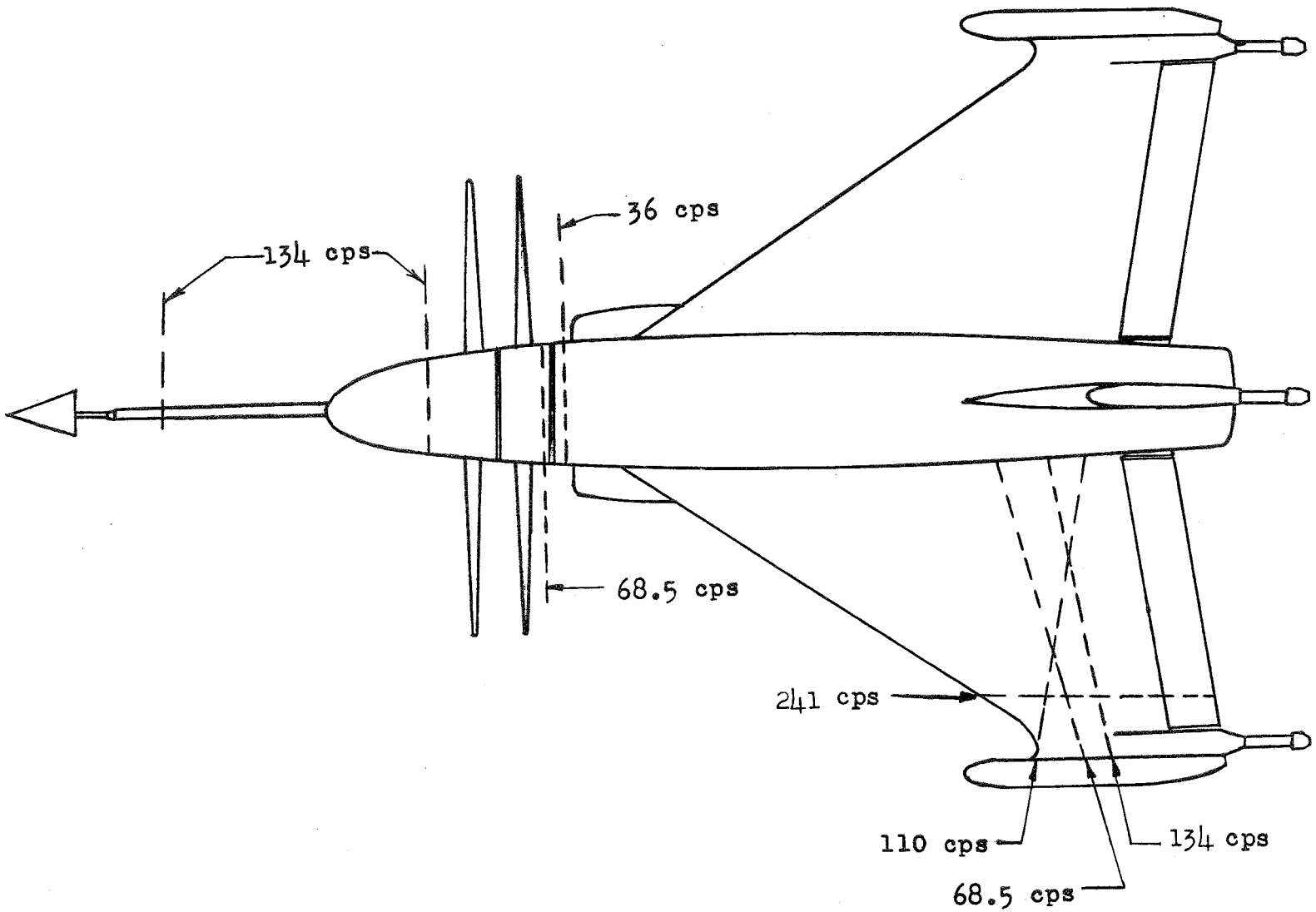

Figure 6.- Node lines at various shaking frequencies.

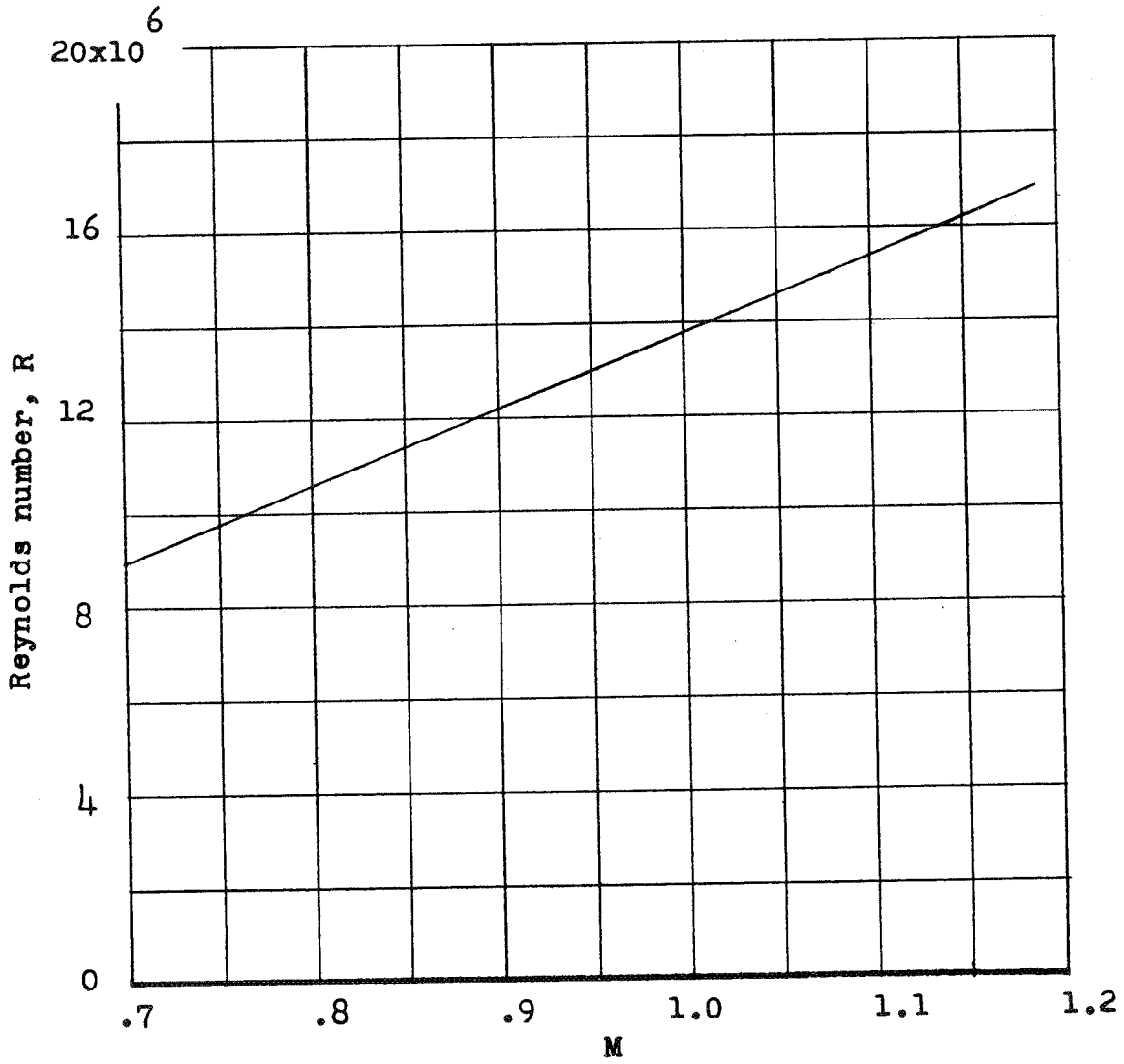

Figure 7.- Reynolds number as a function of Mach number.

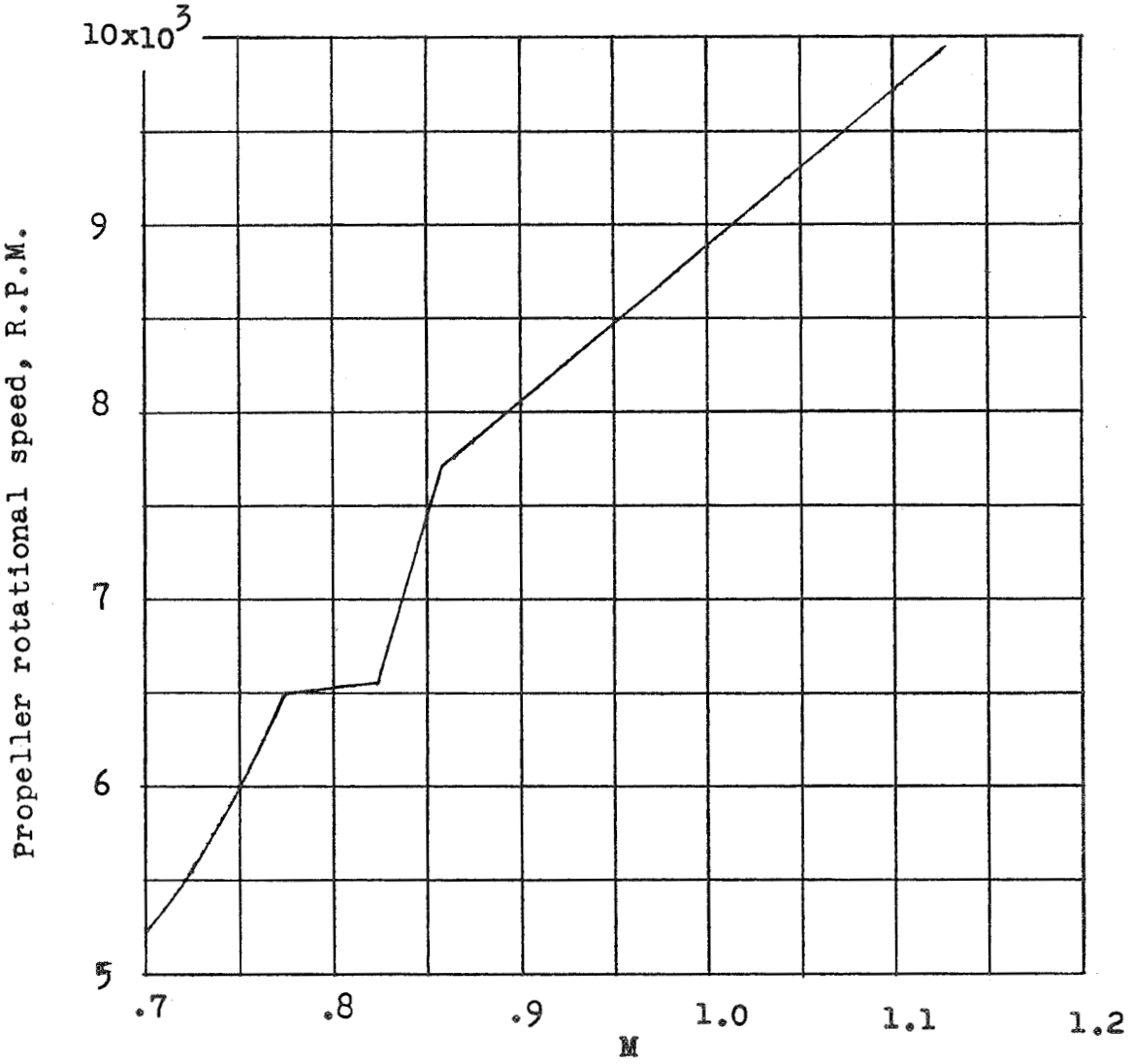

Figure 8.- Propeller windmilling speed as a function of decreasing Mach number. (Curtiss 1058-1059-XC-4 propeller blades at a blade angle of 55°).

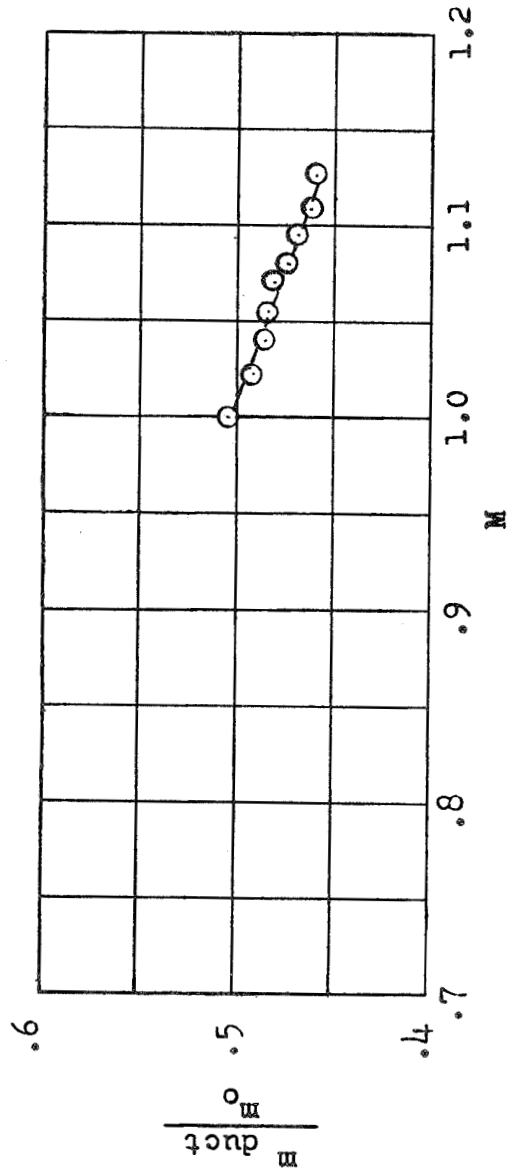

Figure 9.- Duct mass-flow ratio.

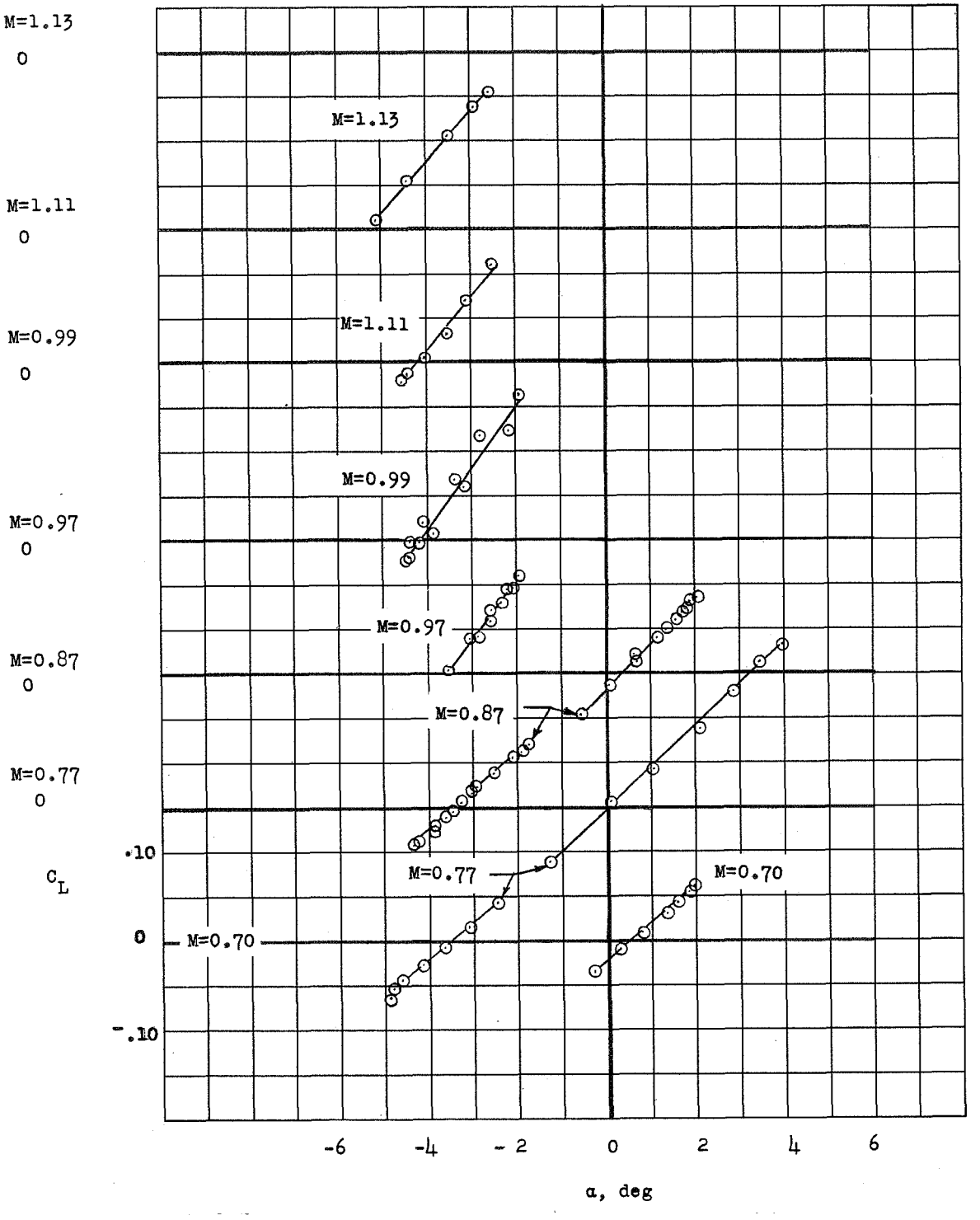

(a) $M > 1.0$, $\delta \approx -1^{\circ}$; $M < 1.0$, $\delta \approx -2^{\circ}$.

Figure 10.- Lift coefficient as a function of angle of attack.

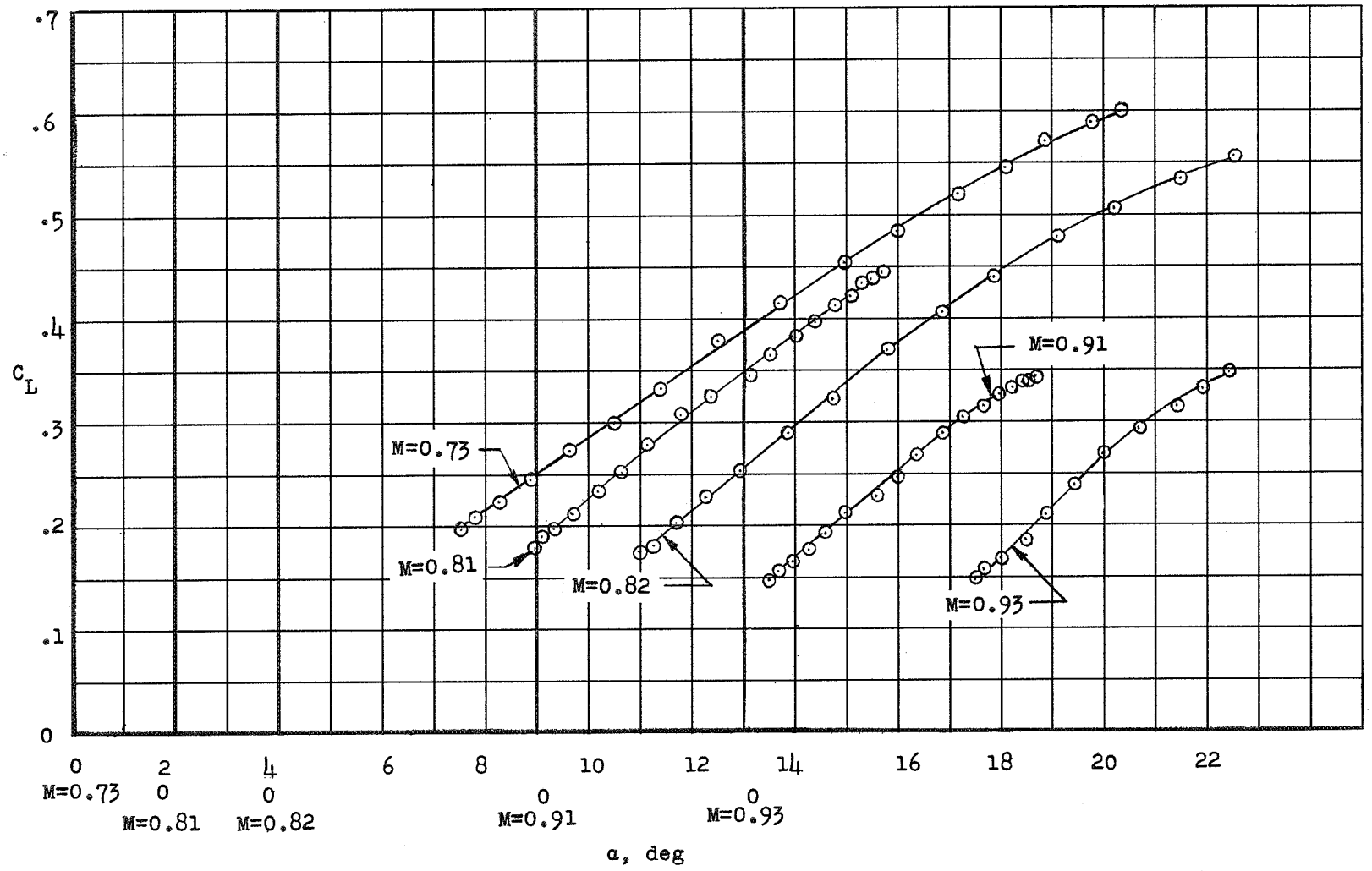

(b) $M > 1.0$, $\delta \approx -6^{\circ}$; $M < 1.0$, $\delta \approx -10^{\circ}$.

Figure 10.- Concluded.

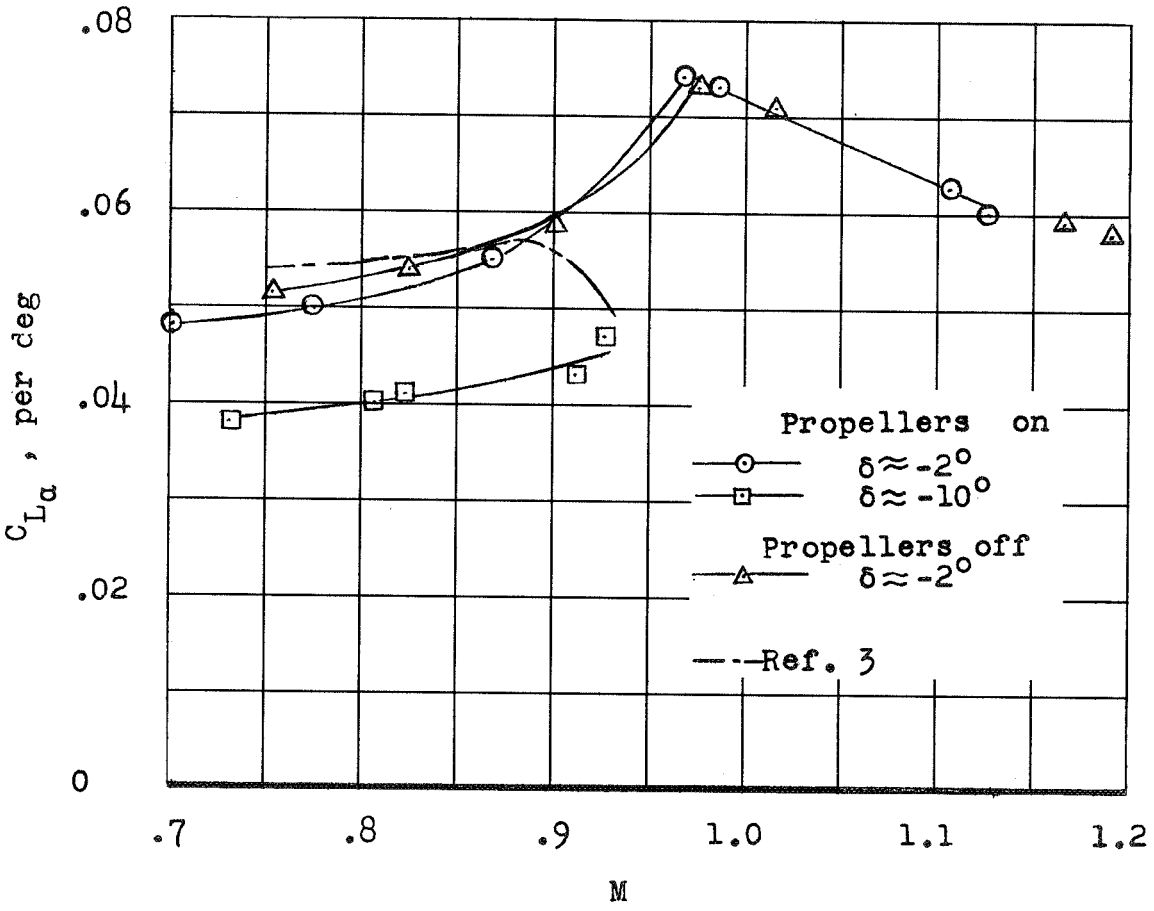

Figure 11.- Variation of lift-curve slope with Mach number.

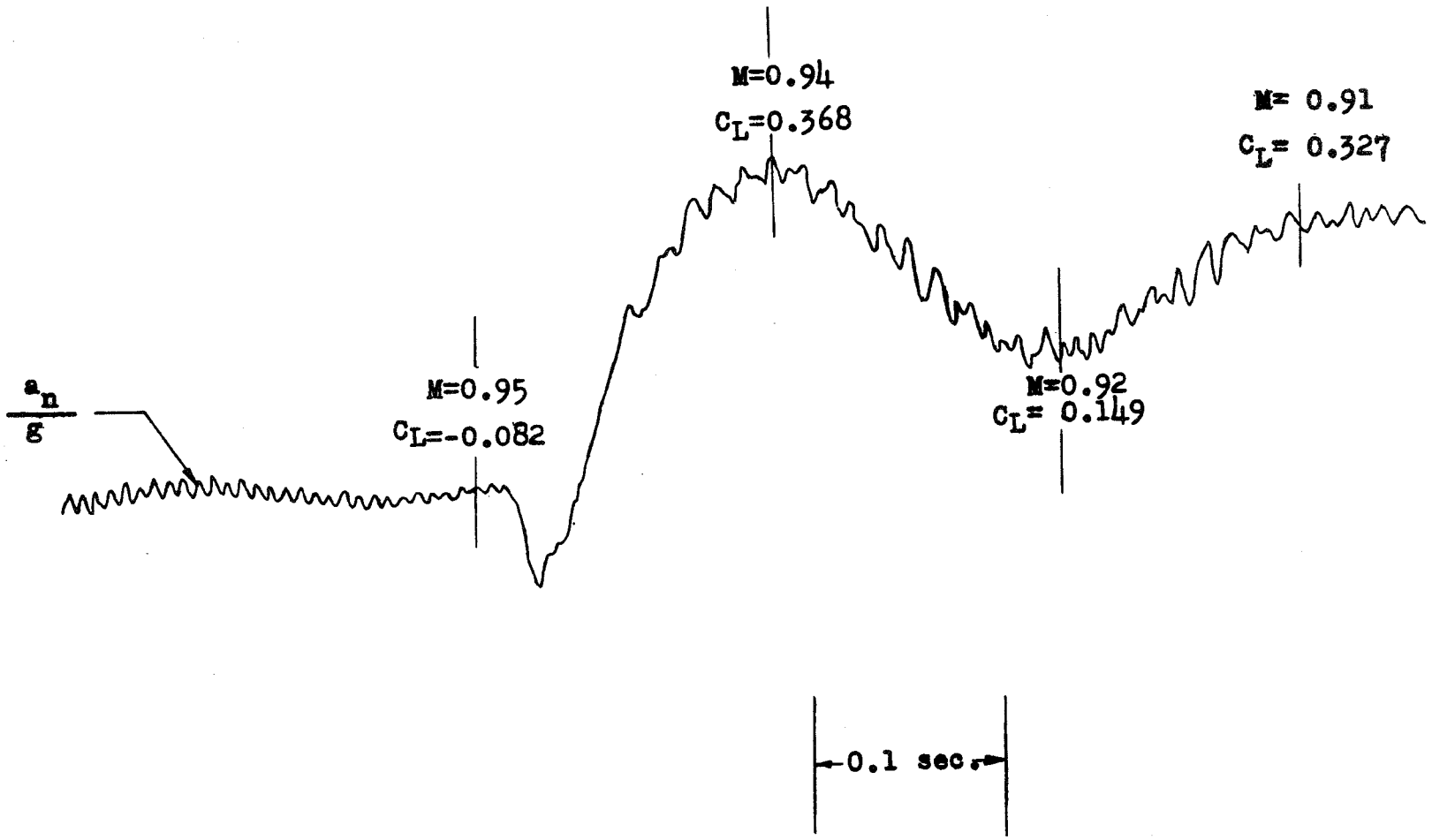

Figure 12.- Section of the telemeter record showing buffet.

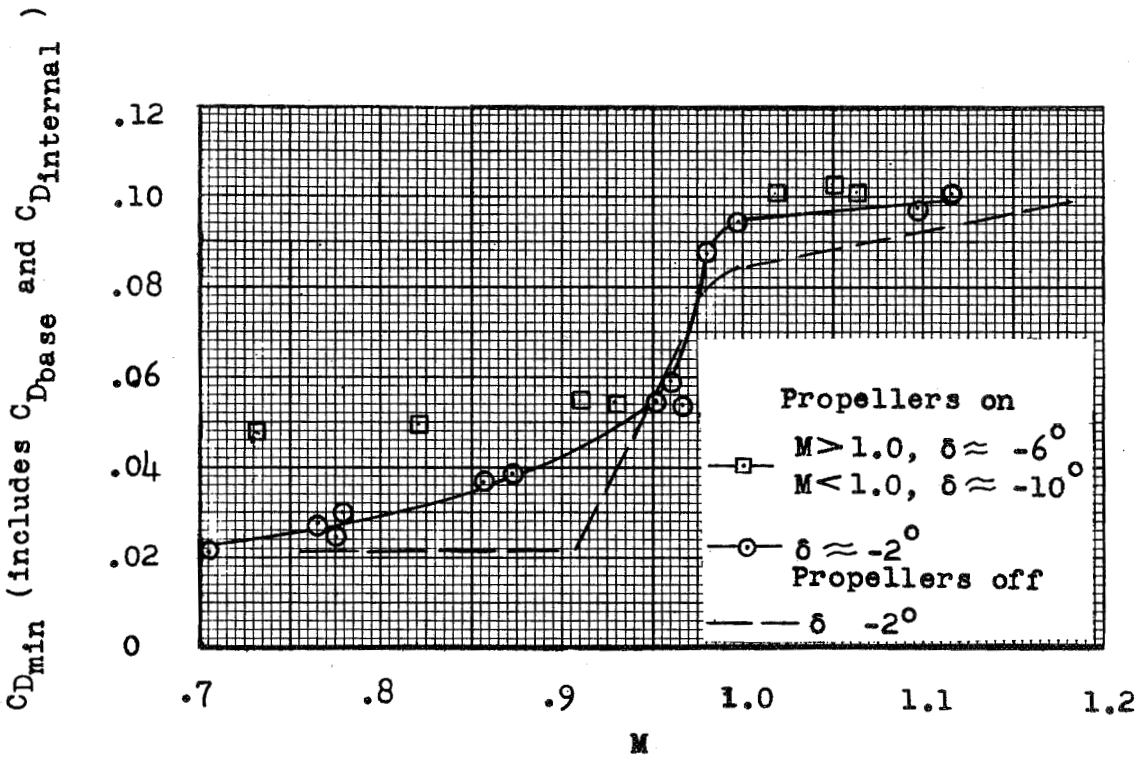

(a) Minimum drag coefficient.

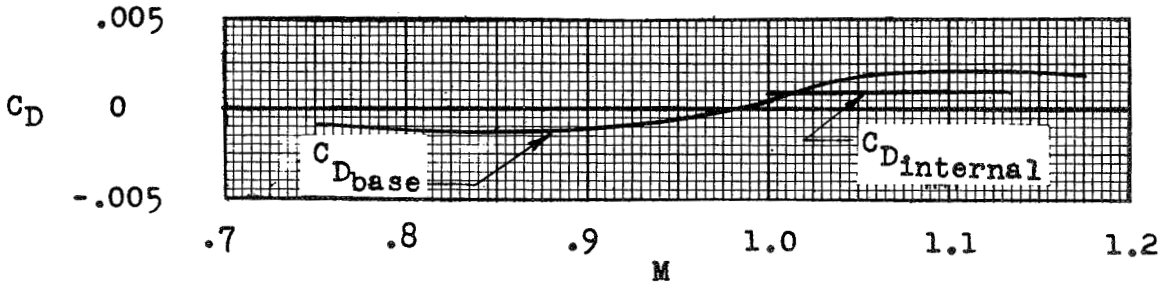

(b) Internal and base drag coefficients.

Figure 13.- Drag coefficient as a function of Mach number.

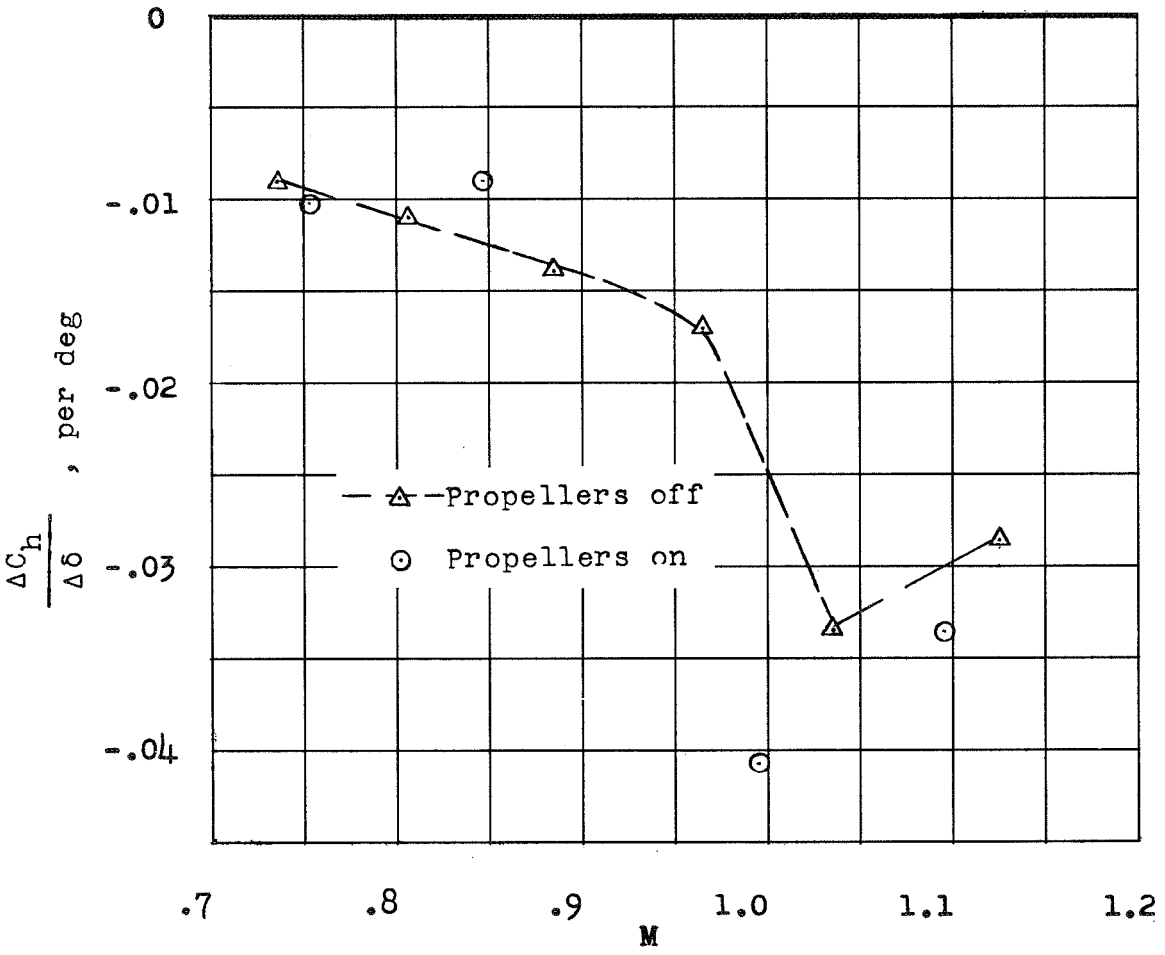

Figure 14.- Effect of Mach number on C_{h_δ}.

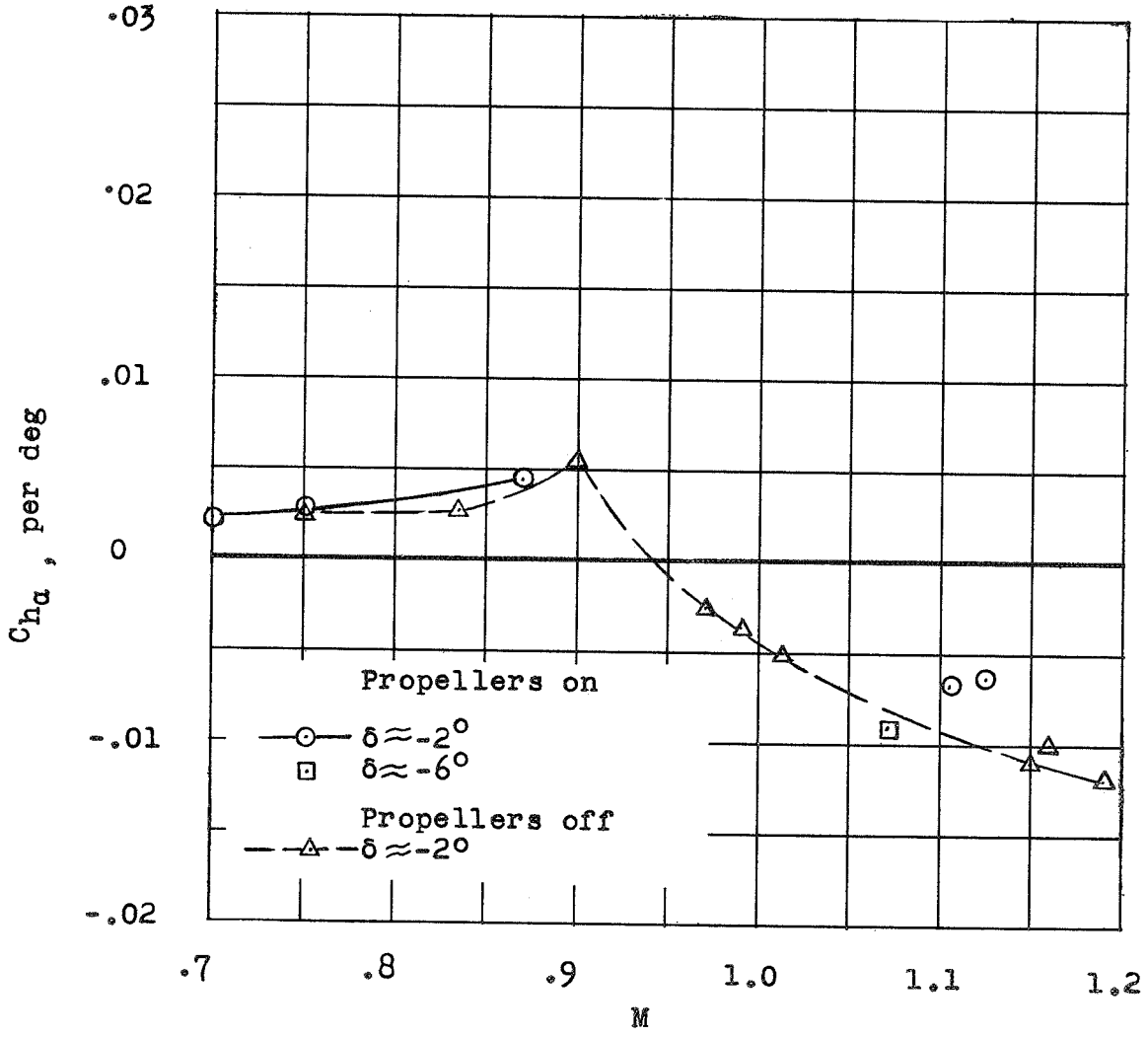

Figure 15.- Effect of Mach number on C_{h_α}.

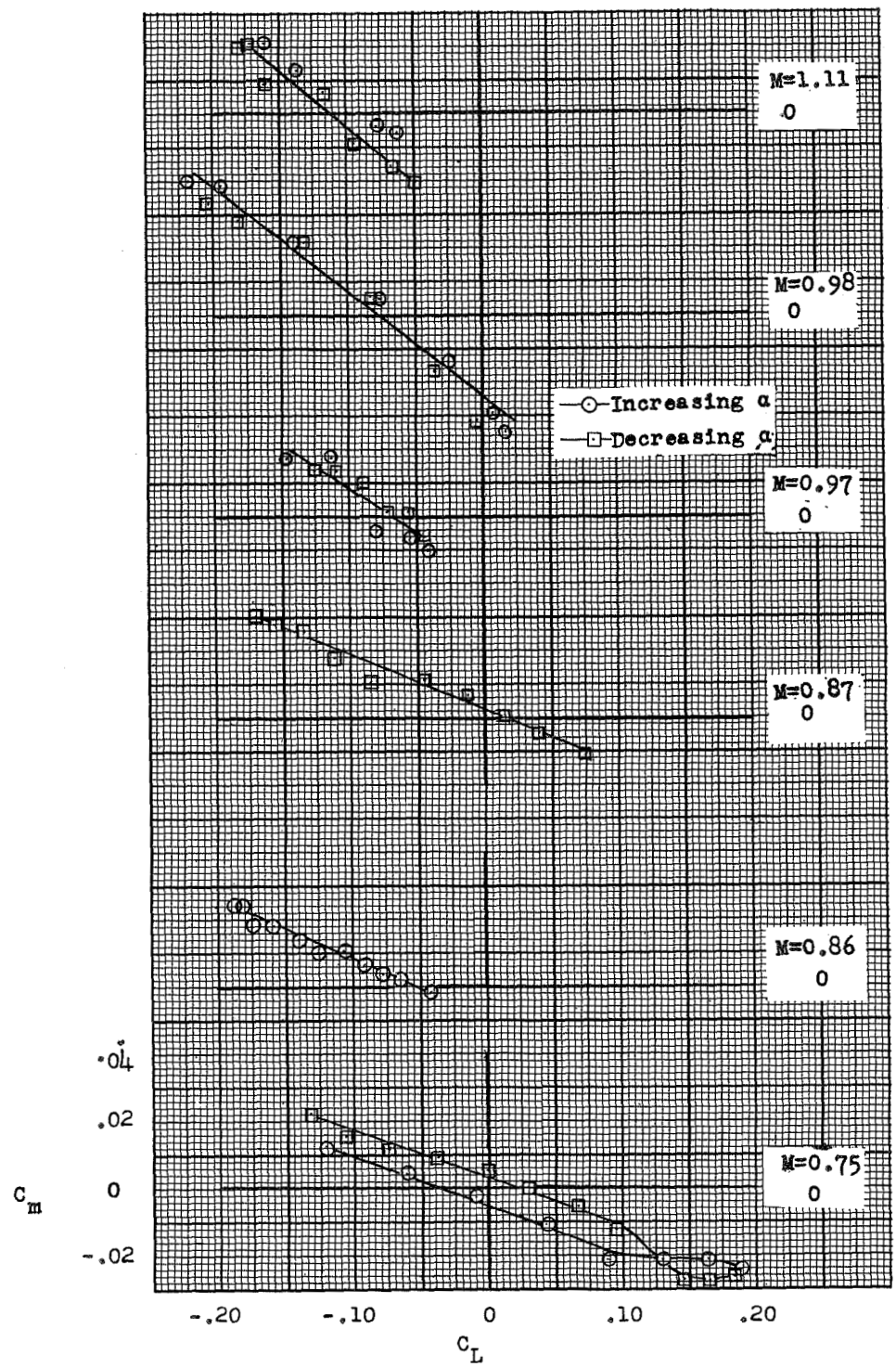

(a) $M > 1.0$, $\delta \approx -1^\circ$; $M < 1.0$, $\delta \approx -2^\circ$.

Figure 16.- Pitching-moment coefficient as a function of lift coefficient. Center of gravity at $0.14\bar{c}$.

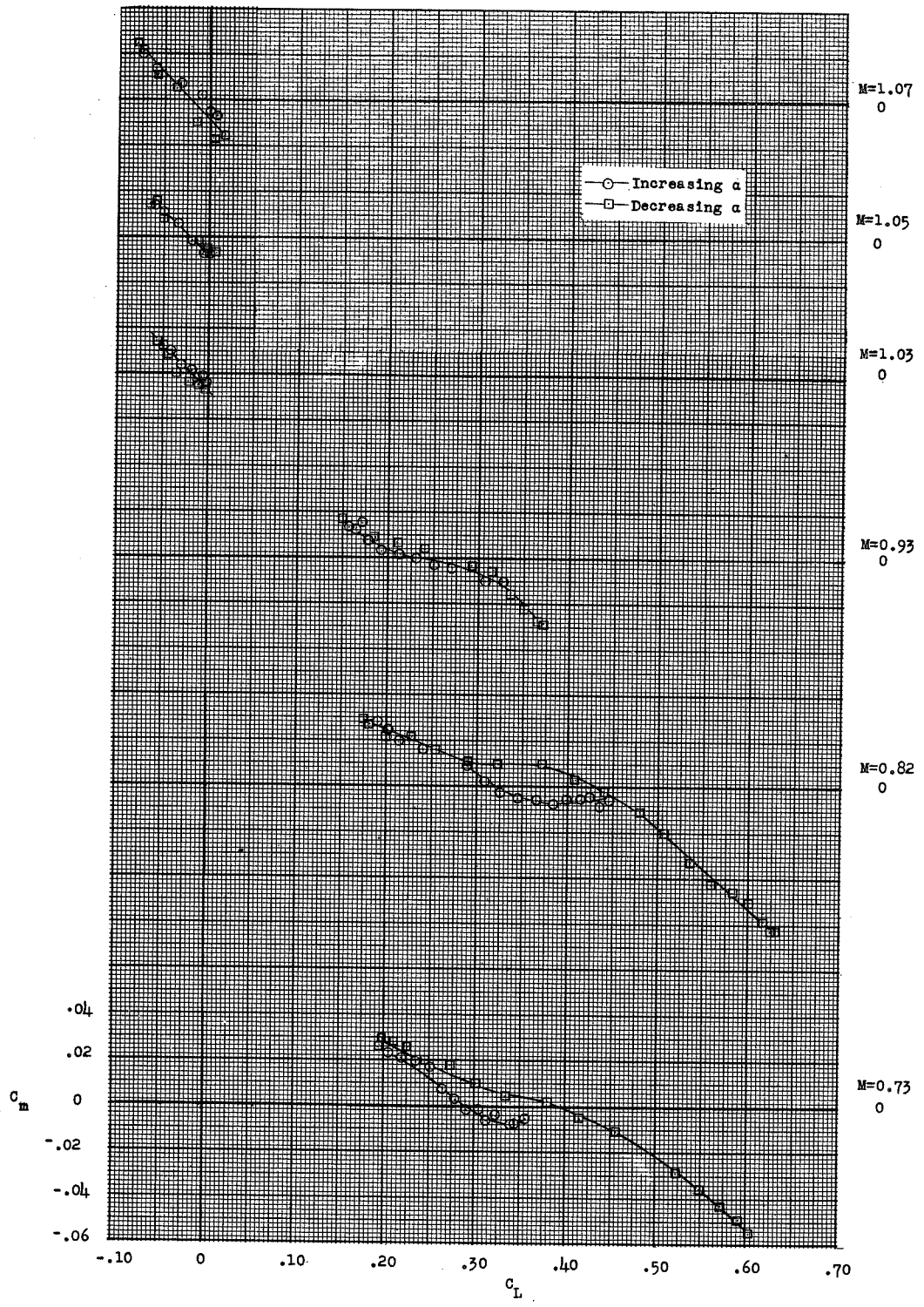

(b) $M > 1.0$, $\delta \approx -6^\circ$; $M < 1.0$, $\delta \approx -10^\circ$.

Figure 16.- Concluded.

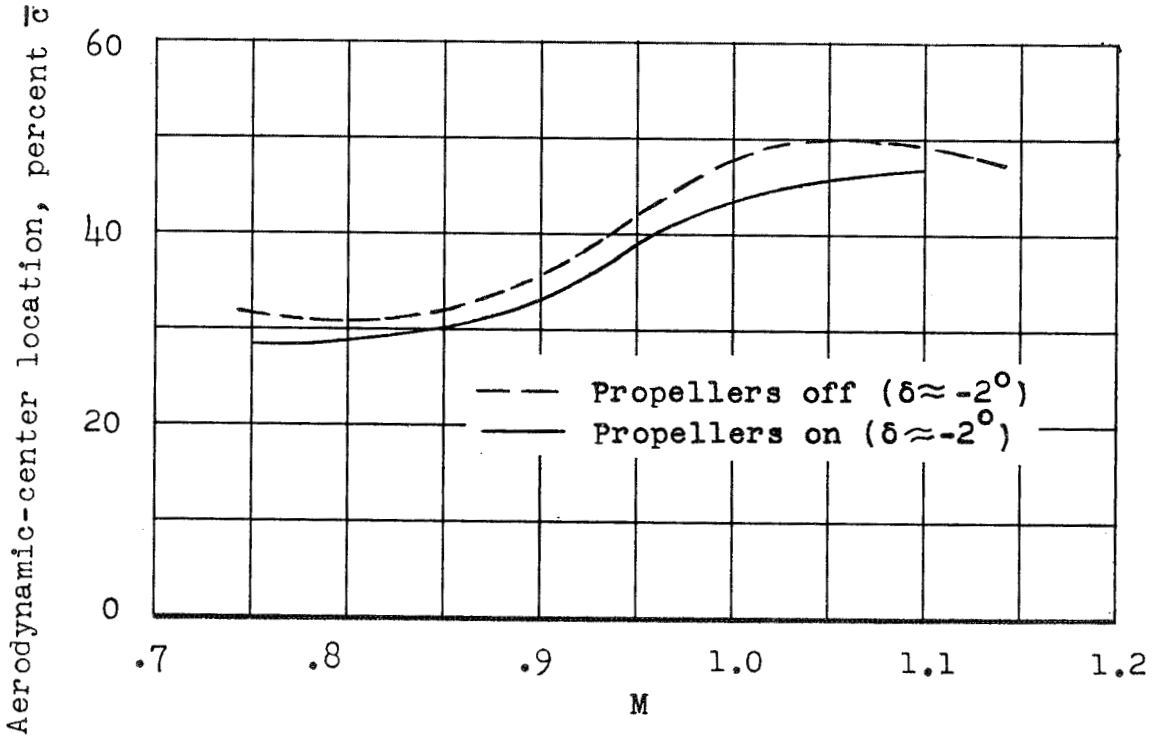

Figure 17.- Aerodynamic-center location as a function of Mach number. ($-0.02 < C_L < 0.10$).

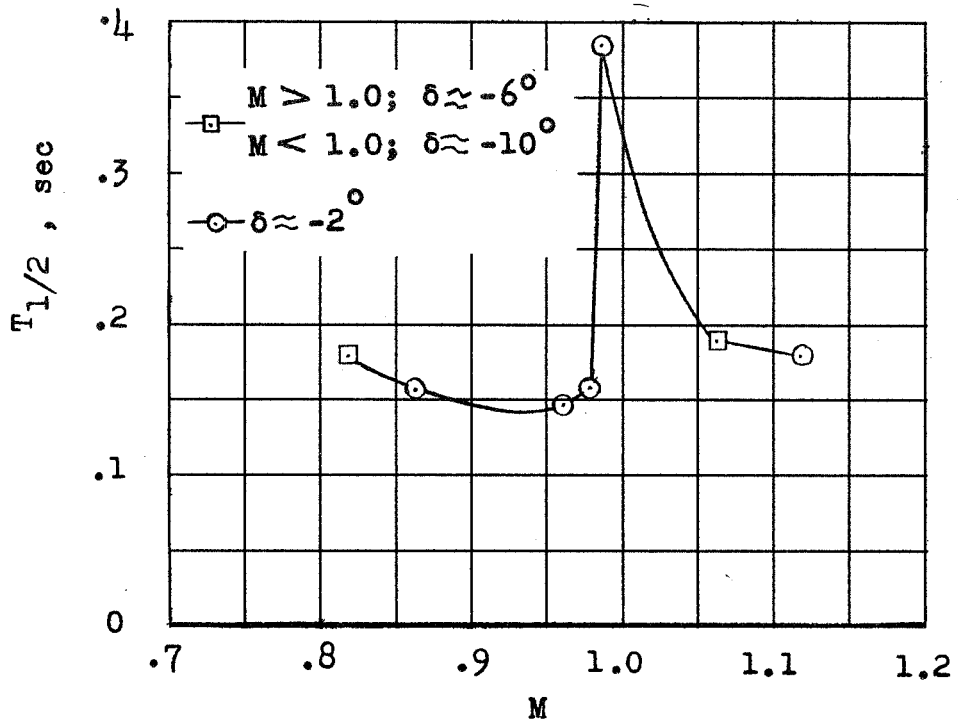

Figure 18.- Time to damp to half amplitude.

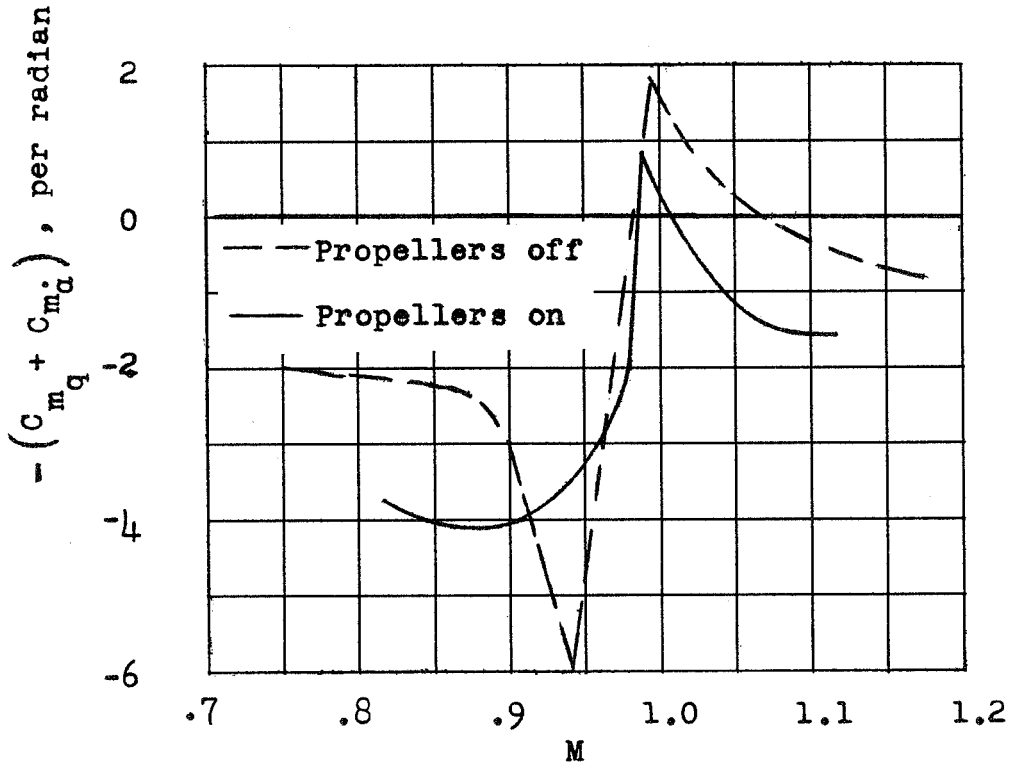

Figure 19.- Pitch-damping parameter. Center of gravity at 0.14$\bar{c}$.

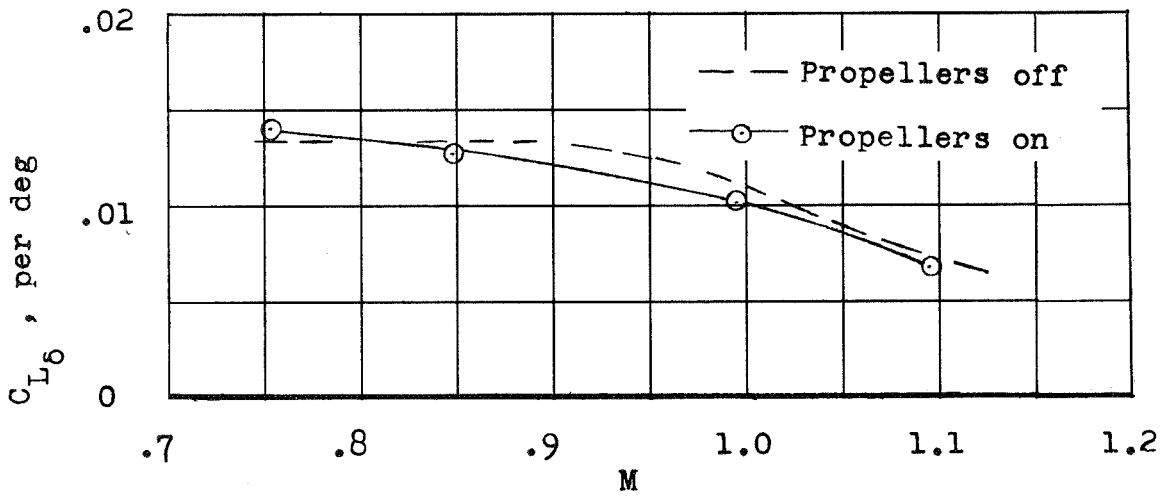

Figure 20.- Control lift effectiveness.

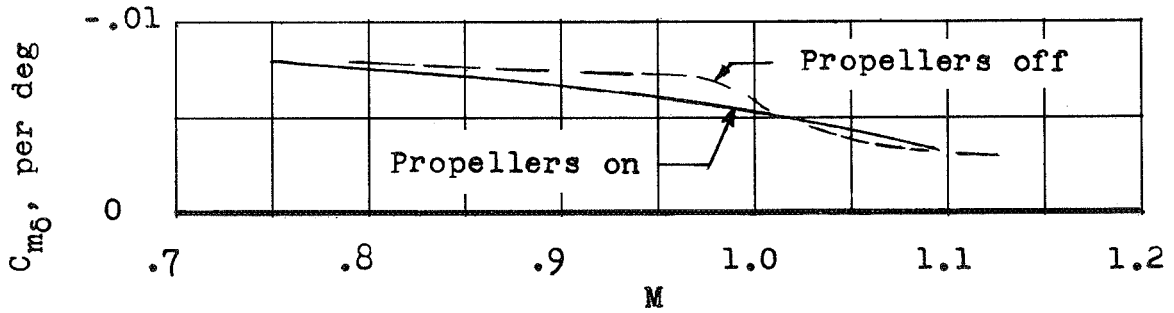

Figure 21.- Control pitching effectiveness. Center of gravity at $0.14\bar{c}$.

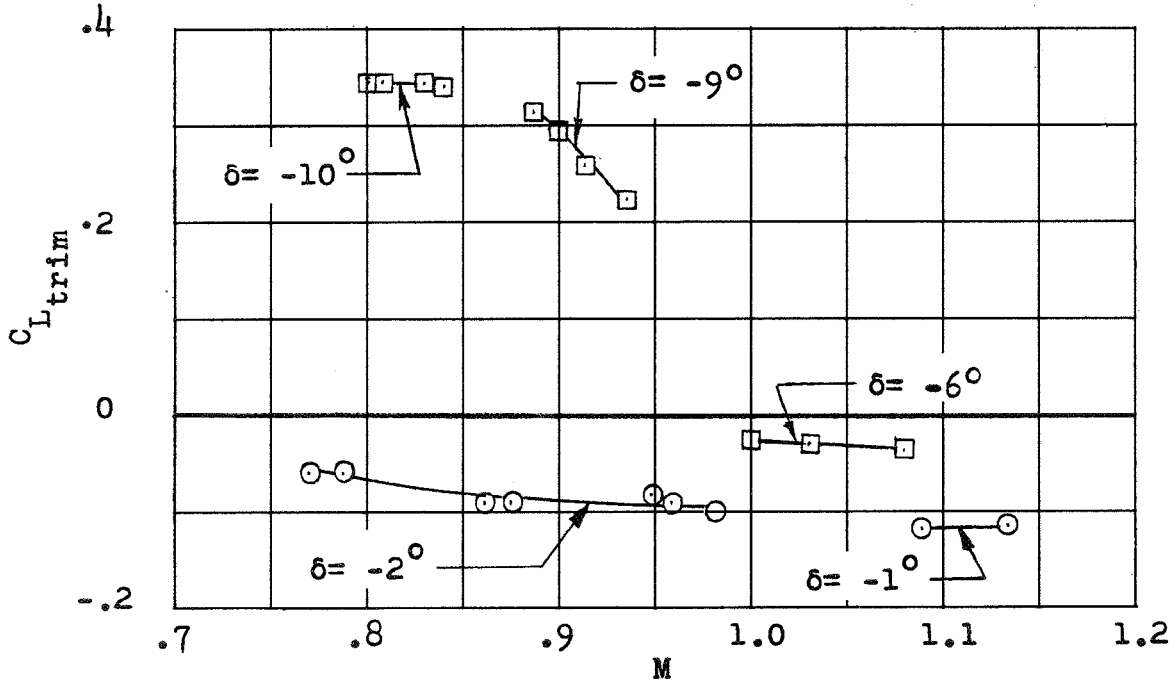

Figure 22.- Trim lift coefficient as a function of Mach number.

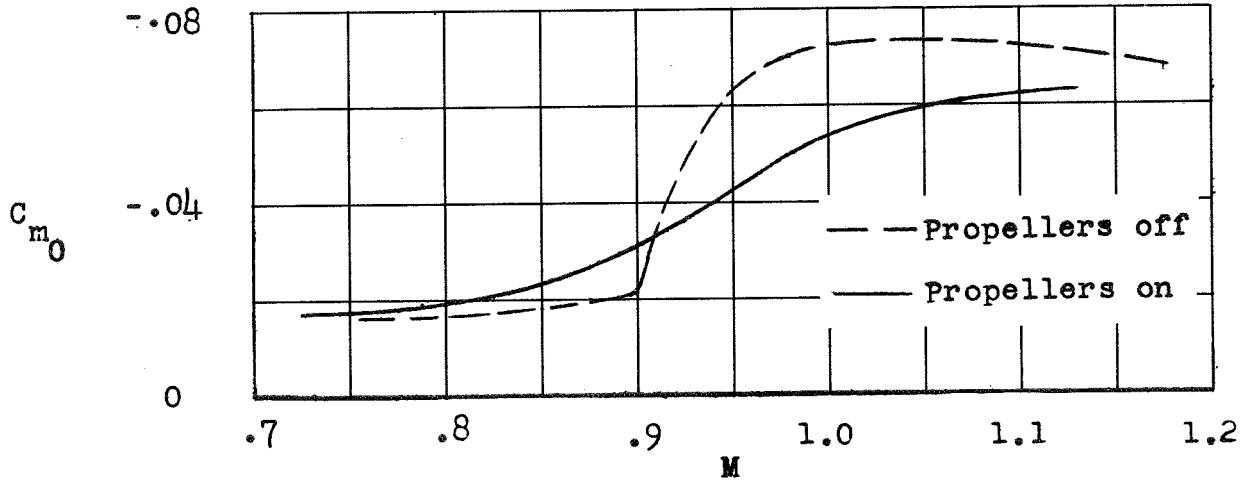

Figure 23.- Basic pitching-moment coefficient. $\alpha = 0^\circ$; $\delta = 0^\circ$.

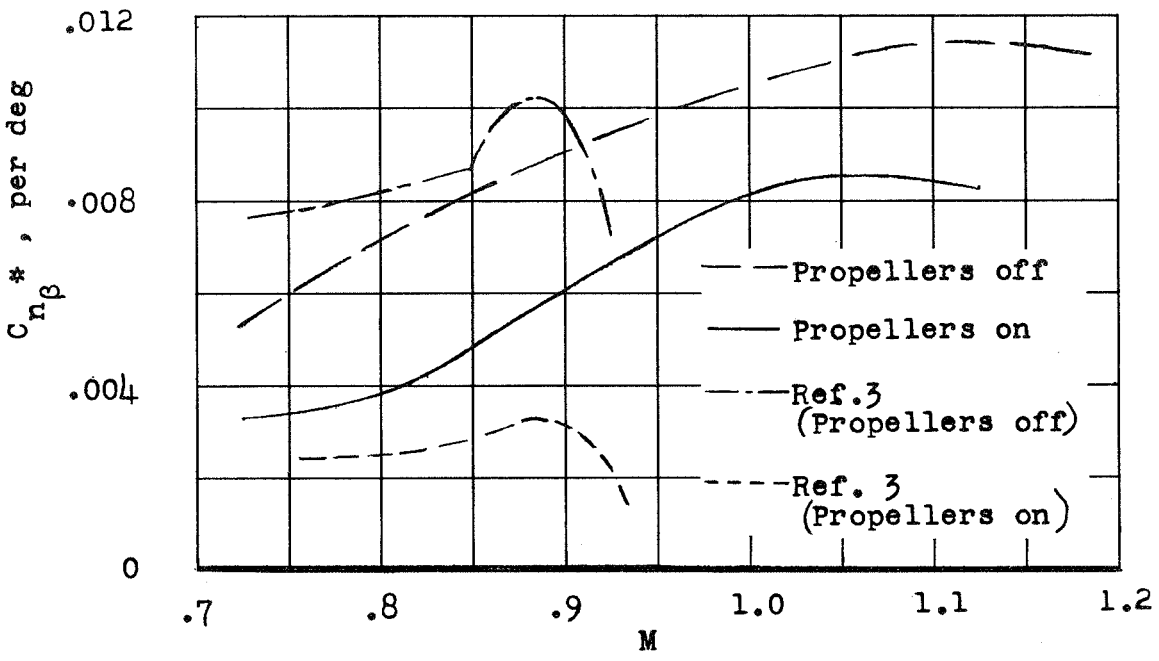

Figure 24.- Effective directional stability parameter as a function of Mach number.

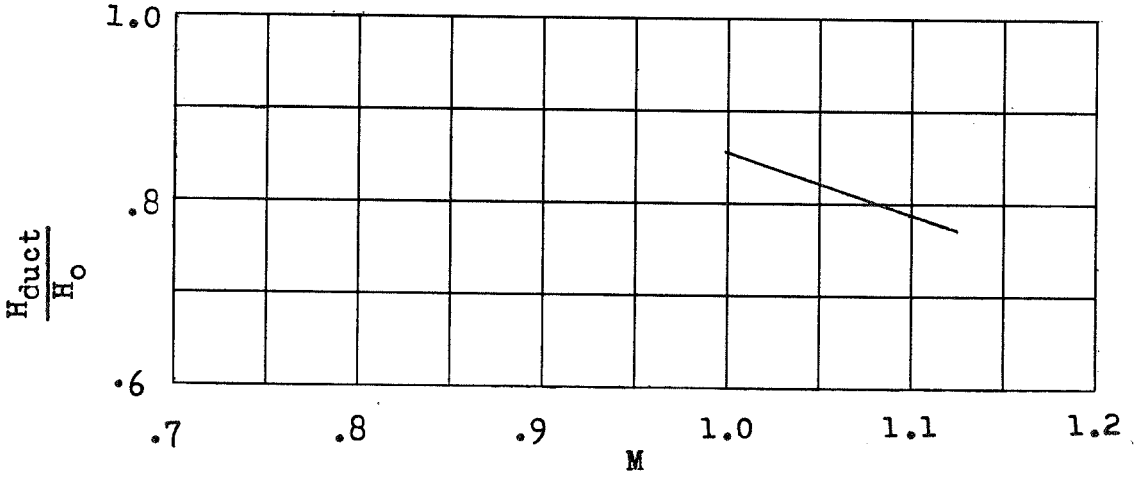

Figure 25.- Duct total-pressure recovery.